Exploring the mesoscale activity in the Solomon Sea: a complementary approach with a numerical model and altimetric data

L. Gourdeau, J. Verron, A. Melet, W. Kessler, F. Marin, B. Djath

AGU PUBLICATIONS

JGR

Journal of Geophysical Research: Oceans

RESEARCH ARTICLE
10.1002/2013JC009614

Special Section:
Western Pacific Ocean Circulation and Climate

Exploring the mesoscale activity in the Solomon Sea: A complementary approach with a numerical model and altimetric data

L. Gourdeau[1], J. Verron[2], A. Melet[1], W. Kessler[3], F. Marin[1], and B. Djath[2]

[1]LEGOS, UMR5566, IRD, Université Paul Sabatier, Toulouse, France, [2]LGGE, UMR5183, CNRS, Université de Grenoble, Grenoble, France, [3]NOAA/Pacific Marine Environmental Laboratory, Seattle, Washington, USA

Key Points:
- A first analysis of the surface mesoscale activity in the Solomon Sea
- Mesoscale is related with the SEC inflow at Solomon Strait rather than to LLWBC
- Maximum activity is in May–June, it is enhanced during La Nina conditions

Correspondence to:
L. Gourdeau,
lionel.gourdeau@legos.obs-mip.fr

Citation:
Gourdeau, L., J. Verron, A. Melet, W. Kessler, F. Marin, and B. Djath (2014), Exploring the mesoscale activity in the Solomon Sea: A complementary approach with a numerical model and altimetric data, *J. Geophys. Res. Oceans*, *119*, 2290–2311, doi:10.1002/2013JC009614.

Received 14 NOV 2013
Accepted 14 MAR 2014
Accepted article online 18 MAR 2014
Published online 14 APR 2014

Abstract The Solomon Sea is an area of high level of eddy kinetic energy (EKE), and represents a transit area for the low-latitude western boundary currents (LLWBCs) connecting the subtropics to the equatorial Pacific and playing a major role in ENSO dynamics. This study aims at documenting the surface mesoscale activity in the Solomon Sea for the first time. Our analysis is based on the joint analysis of altimetric data and outputs from a 1/12° model simulation. The highest surface EKE is observed in the northern part of the basin and extends southward to the central basin. An eddy tracking algorithm is used to document the characteristics and trajectories of coherent mesoscale vortices. Cyclonic eddies, generated in the south basin, are advected to the north by the LLWBCs before merging with stationary mesoscale structures present in the mean circulation. Anticyclonic eddies are less numerous. They are generated in the southeastern basin, propagate westward, reach the LLWBCs, and dissipate. The seasonal and interannual modulations of the mesoscale activity are well marked. At seasonal time scale, maximum (minimum) activity is in May–June (September). At interannual time scale, the mesoscale activity is particularly enhanced during La Niña conditions. If instabilities of the regional circulations seem to explain the generation of mesoscale features, the modulation of the mesoscale activity seems to be rather related with the intrusion at Solomon Strait of the surface South Equatorial Current, rather than to the LLWBCs, by modulating the horizontal and vertical shears suitable for instabilities.

1. Introduction

The Solomon Sea is the last passageway for the South Pacific low-latitude western boundary currents (LLWBCs) before joining the equatorial band (Figure 1). The LLWBCs supply water of subtropical origin to the Equatorial Undercurrent (EUC), Warm Pool, and Indonesian Throughflow [*Tsushiya*, 1989; *Grenier et al*., 2011]. Changes in the strength, pathways, or water mass properties of the LLWBCs are hypothesized to influence Pacific decadal variability and ENSO low-frequency modulation [*Luo and Yamagata*, 2001; *Luo et al*., 2003, 2005; *Nonaka and Sasaki*, 2007]. The possibility that such changes of the LLWBCs might occur in the Solomon Sea has motivated the investigation of the circulation in the Solomon Sea through both modeling and in situ monitoring in the framework of the CLIVAR/Southwest Pacific Ocean and Climate Experiment (SPICE) [*Ganachaud et al*., 2008; A. Ganachaud et al., Ocean circulation of the Southwest Pacific new insights from the Southwest Pacific Ocean and Climate Experiment (SPICE), submitted to *Journal of Geophysical Research: Oceans*, 2014].

The Solomon Sea is a semienclosed basin located north of the Coral Sea bounded on the west by the mainland of Papua New Guinea (PNG), on the east by the Solomon Islands chain (SI), and on the north by the island of New Britain (NB). The complex geography of this basin is at the origin of a double system of LLWBCs, one flowing northward along the PNG coast as the New Guinea Coastal Undercurrent (NGCU), exiting the Solomon Sea via Vitiaz Strait in its northwest corner, and the other turning eastward along NB as the New Britain Coastal Undercurrent (NBCU) [e.g., *Melet et al*., 2010a] to feed the equatorward New Ireland Coastal Undercurrent [*Butt and Lindstrom*, 1994]. As a result, the LLWBCs exit the Solomon Sea through three narrow straits (Vitiaz Strait, St. George's Channel, and Solomon Strait, Figure 1) providing different connecting pathways to the equatorial region. The Solomon Sea is also suspected to be a region of strong vertical mixing. Notably, tidal models point the Solomon Sea as a region of intense generation of internal tides [e.g., *Niwa and Hibiya*, 2001], whose breaking is the main source of turbulent vertical mixing in the ocean

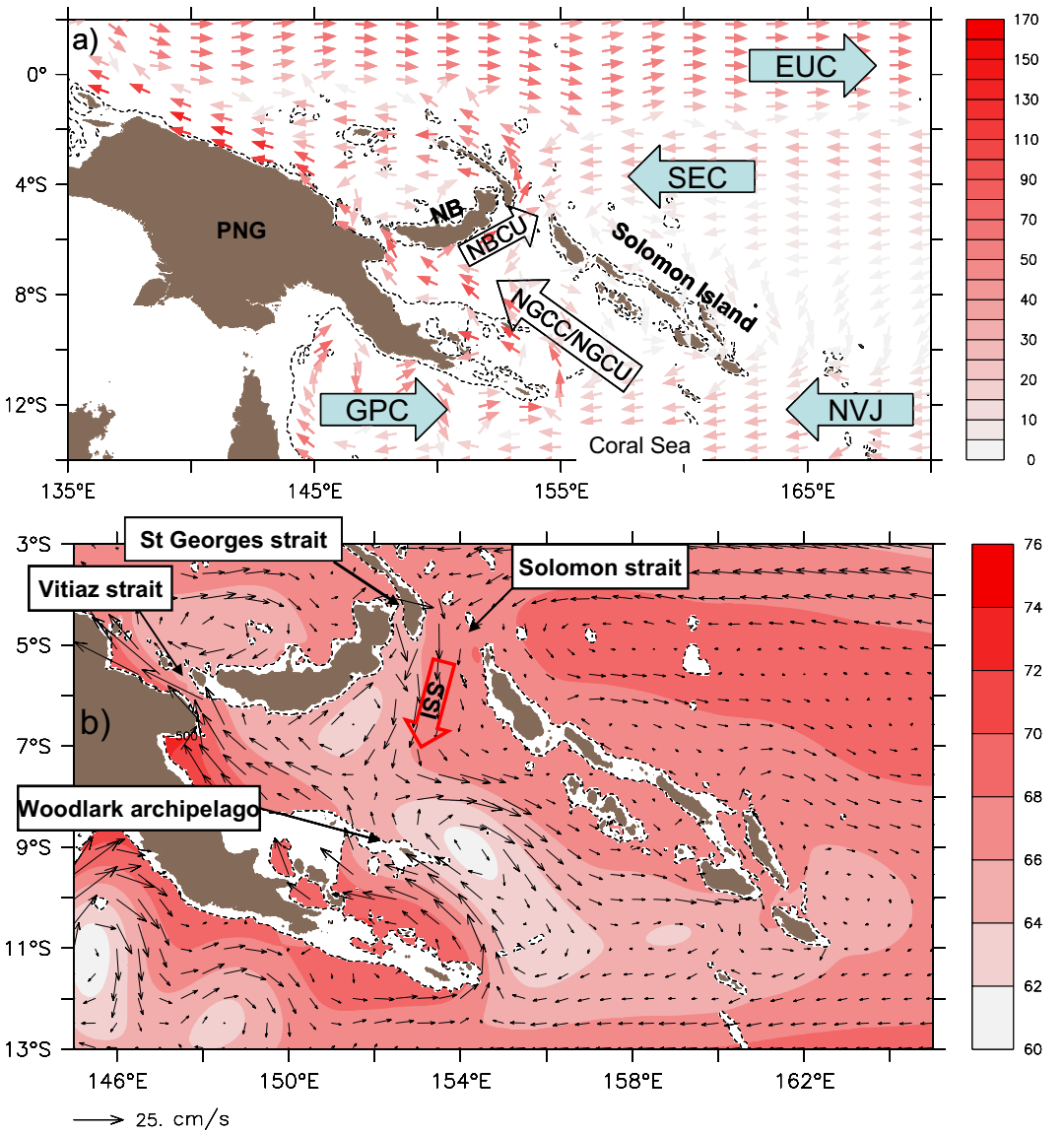

Figure 1. (a) Mean 0–300 m vertically integrated transport (m^2/s) in the southwestern tropical Pacific simulated in the Drakkar ORCA12 simulation. PNG stands for Papua New Guinea and NB for New Britain. The main currents are labeled, including the Gulf of Papua Current (GPC), North Vanuatu Jet (NVJ), the South Equatorial Current (SEC), New Guinea Coastal Current/Undercurrent (NGCC/NGCU), New Britain Coastal Undercurrent (NBCU), Equatorial Undercurrent (EUC). (b) Mean surface geostrophic circulation (black arrows, in m/s, scale given at the bottom) in the Solomon Sea deduced from the simulated sea surface height (shading, in cm). SSI stands for the Solomon Strait Inflow. The dashed line represents the 500 m isobath.

interior [*Garrett and Kunze*, 2007]. In their modeling study, *Melet et al.* [2011] showed that the temperature and salinity of the waters transiting through the Solomon Sea were in better agreement with observations when vertical mixing induced by the dissipation of internal tides was parameterized in their model. Strong diapycnal mixing in the Solomon Sea mostly explained the erosion of the high salinity of upper thermocline water [*Donguy*, 1994], and its export toward surface and deeper layers. Finally, the LLWBC pathways, strengths, and water mass modifications in the Solomon Sea all vary at ENSO time scales [*Melet et al.*, 2013].

Until now, studies of the Solomon Sea have mainly focused on the mean circulation and its seasonal and interannual variability [*Melet et al.*, 2010a, 2010b, 2011, 2013; *Cravatte et al.*, 2011; *Hristova and Kessler*, 2012; *Davis et al.*, 2012]. However, mesoscale activity could also significantly impact the thermodynamical characteristics of Solomon Sea waters joining the equatorial region. The mesoscale activity could be an important

mechanism for transporting and mixing water properties in this region, as suggested by *Melet et al*. [2013]. Phenomenological representations of mesoscale activity include eddies or isolated vortices, and current meanders which in turn can produce fronts, squirts, and filaments where mixing can be enhanced. They usually refer to a subclass of energetic motions with typical space and time scales of 50–500 km and 10–100 days [*Le Traon and Morrow*, 2001]. In the global ocean, the kinetic energy of ocean circulation is dominated by mesoscale eddies, which play a significant role in transporting water mass, heat, and nutrients [*Roemmich and Gilson*, 2001]. Their characteristics have been largely documented, especially from altimetry [*Stammer*, 1998; *Fu*, 2009; *Chelton et al*., 2011]. Semienclosed marginal seas are particular areas where eddy generation and their dynamics are highly constrained by the topography. An abundant literature exists on the mesoscale eddies in the marginal South China Sea (SCS) documenting eddy formation and properties as well as their impact on the thermohaline structure [e.g., *Hwang and Chen*, 2000; *Wang et al*., 2003, 2008; *Zheng et al*., 2011; *Nan et al*., 2011]. In the marginal Caribbean Sea, the high mesoscale activity is mostly linked with instabilities of the local currents and is modulated by the possible intrusion of the North Brazil Current rings, and the transmission of Rossby waves through ocean barriers such as the Lesser Antilles [*Jouanno et al*., 2009; *Simmons and Nof*, 2002; *Pedlosky*, 2000]. Regarding the marginal semienclosed Solomon Sea, some insight into the mesoscale activity has been recently gained from the analysis of altimetric [*Melet et al*., 2010b] and in situ glider data [*Davis et al*., 2012], but it has thus far not been the focus of a specific study.

This paper aims to explore and characterize the mesoscale activity in the Solomon Sea for the first time. We develop a complementary approach based on the joint analysis of an eddy-resolving ocean general circulation model (OGCM) and altimetric data. Altimetry provides a long time series of synoptic maps of dynamic topography (DT) and is therefore useful to analyze the mesoscale activity at the surface. A tracking eddy procedure based on the DT fields is used to document their characteristics. Since the model is consistent with altimetric data regarding mesoscale activity in the Solomon Sea, it is used to provide some insights on the vertical distribution of eddy kinetic energy (EKE) and on the possible dynamical processes at play.

The paper is organized as follows: section 2 provides some details on the numerical simulation and data used in this study, section 3 focuses on the EKE signal, its variability, and its spatial distribution, section 4 investigates mesoscale eddies, their mean features, and their seasonal and interannual variability. Finally, results are summarized in section 5.

2. Model and Data

2.1. Model

2.1.1. Description

To study the mesoscale activity in the Solomon Sea from an OGCM, the model has to properly resolve the corresponding dynamical scales (i.e., be eddy-resolving). In the Solomon Sea, the deformation radius of the first baroclinic mode is in a 100–230 km range [*Chelton et al*., 1998]. A rule of thumb for numerical models is that eight grid points are needed to properly resolve dynamical features [*Marchesiello et al*., 2011]. Therefore, a resolution of at least 1/12° is required to properly resolve the mesoscale eddies in the Solomon Sea.

In this study, we analyze the ORCA12.L46-MAL95 configuration of the global 1/12° OGCM developed and operated in the DRAKKAR consortium [*Lecointre et al*., 2011]. This model is based on OPA, the ocean physical component of the NEMO ocean modeling system [*Madec et al*., 2008]. NEMO-OPA resolves the classic primitive equations on a sphere, discretized on an Arakawa C grid with a Mercator projection. Geopotential vertical coordinates are used with 46 levels with 6 m resolution in the upper layers and down to a 250 m resolution in the deepest regions (5750 m). The "partial step" approach [*Adcroft et al*., 1997] is used to allow the bottom cells' thickness to be modified to fit the local bathymetry: this approach improves the representation of topographic effects [*Barnier et al*., 2006; *Penduff et al*., 2007]. The bathymetry was built from the GEBCO1 data set (http://www.gebco.net/data_and_products/gebco) for regions shallower than 200 m and from ETOPO2 (www.ngdc.noaa.gov/mgg/global/relief/ETOPO2) for regions deeper than 400 m (with a combination of both data sets in the 200–400 m depth range). Lateral boundary conditions have a strong impact on the stability of boundary currents [*Verron and Blayo*, 1996; B. Djath et al., A 1/36° model of the Solomon Sea embedded into a global ocean model: On the setting up of an interactive open boundary condition nested model system, in revision for the *Journal of Operational Oceanography*, 2014].

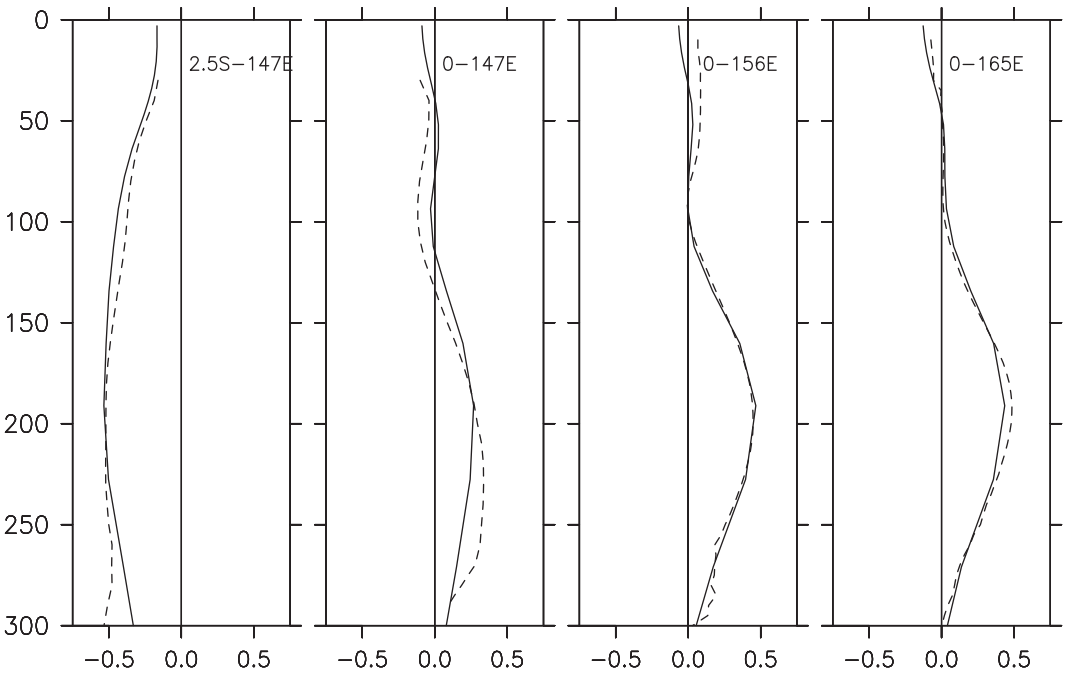

Figure 2. Comparison of the 1989–2011 mean current vertical profiles (in m/s) simulated by the model (continuous line) and observed from the TAO moorings (dashed line) along the equator and at 2.5°S–142°E.

A weak partial-slip condition is used that is between the "free-slip" (the coastal vorticity is set to 0) and the "no-slip" (the tangential velocity is set to 0) conditions. The atmospheric forcing (both mechanical and thermodynamical) is applied to the model using the CORE bulk-formulae approach [*Large and Yeager*, 2004, 2009].

The simulation started from rest in 1978 with initial conditions for temperature and salinity provided by the World Ocean Atlas 1998 [*Levitus*, 1998]. It was spun up for 11 years using the CORE-II interannual forcing data set and then integrated from 1989 to 2007 using an ERA-interim derived forcing. The 3-D ocean state (temperature, salinity, and velocities), and the 2-D sea surface height (SSH) are saved as 5 day means during the period of integration.

2.1.2. Evaluation

Recent observational work on the Solomon Sea circulation from SPICE-related studies [*Melet et al*., 2010b; *Cravatte et al*., 2011; *Hristova and Kessler*, 2012] helped evaluate this simulation over the southwest Pacific region. The Solomon Sea circulation strongly depends on the main sources of the currents feeding it: these include the Gulf of Papua Current (GPC) [*Ganachaud et al*., 2012], the North Vanuatu Jet (NVJ), and the South Equatorial Current (SEC) (Figure 1). The LLWBCs (NGCU and NBCU) flow at thermocline level. They are overlaid by highly variable currents in the surface layer: the New Guinea Coastal Current (NGCC), the NVJ, and the intrusion of the SEC at Solomon Strait named here the Solomon Strait Inflow (SSI) for convenience. SSI is southwestward in the northern Solomon Sea basin and turns southeastward in the southern basin. The pathway of the LLWBCs in the Solomon Sea at thermocline level in the present solution is clearly improved compared to the regional model simulation of *Melet et al*. [2010a] because of the choice of the "partial-slip" boundary condition. Indeed, it allows the strong NGCU to separate from the PNG coast and to bifurcate south of the New Britain Island to become the NBCU in better agreement with observations [*Cravatte et al*., 2011]. The intrusion of the SSI may extend into the central Solomon Sea as observed in *Hristova and Kessler* [2012]. In section 3, it is shown that the SSI is a trigger of mesoscale activity in the Solomon Sea.

The skill of the model in the Solomon Sea can also be assessed by evaluating the realism of the remote western equatorial currents. Indeed, the South Pacific LLWBCs are the main contributors to the EUC [*Tsuchiya et al*., 1989; *Grenier et al*., 2011] and the partition of the LLWBCs through the narrow straits of the Solomon Sea partly conditions the equatorial Pacific currents. The simulated mean vertical profiles of zonal

velocity compare well with observations from the TAO moorings (www.pmel.noaa.gov/tao) located along the equator at 147°E, 156°E, and 165°E, and at 2.5°S–142°E [*Ueki et al*., 2003] even in the far western equatorial Pacific where many OGCMs exhibit biases (Figure 2). *Grenier et al*. [2011] evaluated the same model at a coarser resolution (1/4°) against TAO velocity data and showed some inconsistency in the far western equatorial Pacific [*Grenier et al*., 2011, Figure 2].

Therefore, this eddy-resolving model that has benefited of the pioneer work of *Melet et al*. [2010a] appears well enough realistic with regard to the Solomon Sea circulation, and also with regard to mesoscale activity, as confirmed in the next sections.

2.2. Altimetric Data

Satellite altimetry has emphasized mesoscale activity as the dominant signal in the ocean circulation. Indeed, mesoscale eddies are responsible for most of the altimetric-derived kinetic energy [*Stammer*, 1998]. Altimetric data have been of great benefit to highlight the ubiquitous presence and role of mesoscale eddies in the open ocean [*Morrow et al*., 2004; *Fu*, 2009; *Chelton et al*., 2011] as well as in marginal seas such as the South China Sea or the Caribbean Sea [*Carton and Chao*, 1999; *Nan et al*., 2011], or to provide a benchmark for different theories of ocean turbulence [*Le Traon et al*., 2008; *Xu and Fu*, 2011].

In this study, we use the gridded altimetric data set produced by Ssalto/Duacs and distributed by AVISO, with support from the CNES (http://www.aviso.oceanobs.com/duacs/) over the November 1992 to December 2011 period. This product combines data from up to four altimetry satellites depending upon time (Jason1-2, Envisat or ERS1-2, Topex/Poseidon, and Geosat Follow On). Combining data from different missions significantly improves estimations of mesoscale signals [*Pascual et al*., 2006]. A mapping procedure based on optimal interpolation with realistic correlation functions was applied to produce maps of sea level anomaly (SLA) on a 1/3 × 1/3° grid every week (REF). The complex geography of the Solomon Sea with numerous islands can induce spurious results due to the mapping procedure. Indeed, data were often interpolated over islands that separate distinct dynamical regimes (such as the New Britain Island or the Solomon Islands chain). Despite this limitation, gridded AVISO data were able to provide useful information to understand the seasonal and interannual variability in the Solomon Sea [*Melet et al*., 2010b].

SLA was referenced to the MDT_CNES-CLS09 mean ocean dynamic topography [*Rio et al*., 2011] to get absolute measurements of the ocean dynamic topography (DT). If the sea surface variability inferred from DT and SLA data is identical, using DT instead of SLA data is beneficial to consistently compare altimetric observations with the modeled SSH. Although it is challenging to produce a high-quality mean dynamic topography product in this complex region, it compares well enough with the time-averaged model SSH (not shown). In particular, it exhibits two cyclonic structures: one is located in the northern basin south of New Britain (6.5°S–152°E), and the second one is located at the eastern extremity of the Woodlark Archipelago (9°S–154°E) (Figure 1b). Therefore, the use of DT data is further motivated by the fact that such mean structures have a size typical of mesoscale features. Such apparently permanent structures need to be distinguished from the mesoscale variability of interest in the present study.

To more specifically focus on the analysis of the eddy kinetic energy (section 3), altimetric data were processed to suppress low-frequency variability. Indeed, the large-scale and low-frequency atmospheric forcing at these latitudes induces a circulation response throughout the Solomon Sea at seasonal and interannual time scales. This low-frequency variability is responsible for up to 80% of the altimetric signal variance as revealed by the dominant first two EOF modes calculated from the DT maps (not shown) [e.g., *Melet et al*., 2010b]. Therefore, this low-frequency variability must be filtered out. Since the large-scale variability signal is very well extracted from the EOF analysis, we chose to remove these two dominant EOF modes from the raw signal instead of using a high-pass filter, as is commonly done to extract the intraseasonal variability. The effect of this processing is illustrated in Figure 3. The raw data exhibits relatively low variability in the western side of the basin whereas high variability (up to 16 cm rms) is located in two patches in the eastern Solomon Sea. These two patches are mesoscale and low frequency. It means that in a small basin like the Solomon Sea mesoscale is not necessarily associated with high frequency. The high-frequency DT variability has a different pattern: it extends across the central Solomon Sea with amplitude of 4–5 cm rms. It should

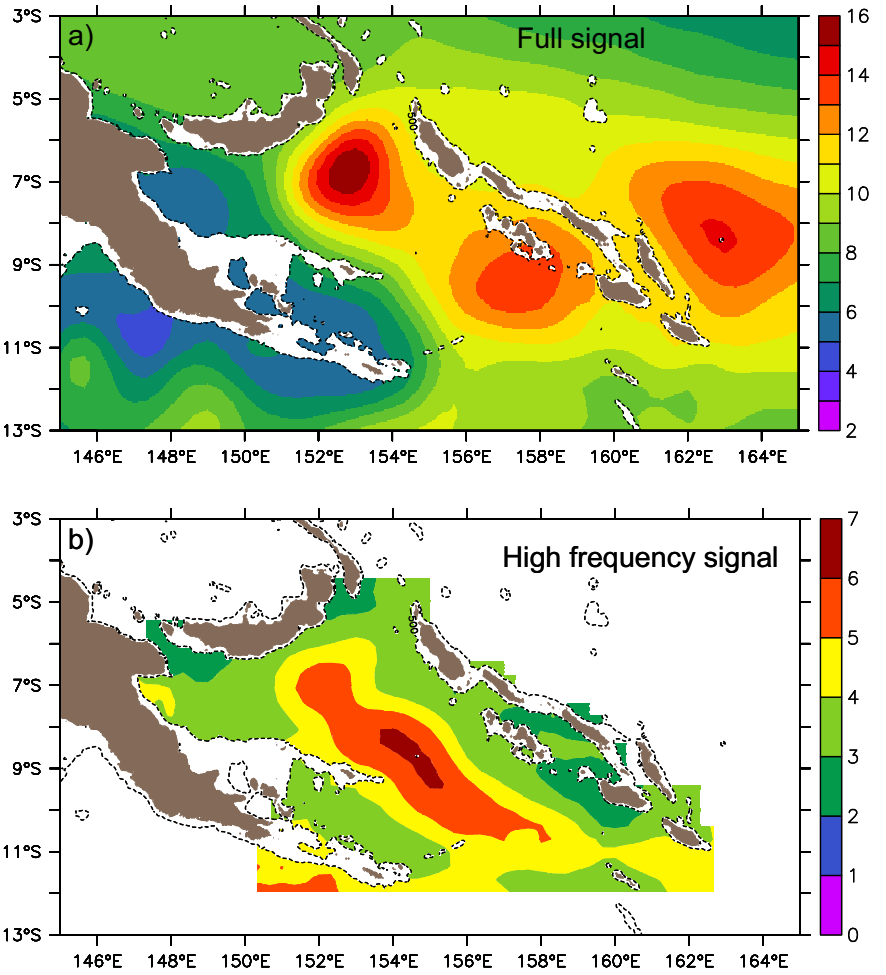

Figure 3. Sea level variability (in cm rms) over the 1993–2011 period from the AVISO gridded data for the (a) full signal, (b) the high-frequency signal where the seasonal and interannual basin scale variability have been filtered out. Note the different colorbars.

be noted that the same data processing applied to the modeled SSH provides a similar SSH variability (not shown).

3. Statistical Description of the Mesoscale Variability

This section provides a statistical description of the mesoscale variability in the Solomon Sea. Mesoscale activity is represented here by the level of eddy kinetic energy (EKE). Altimetric-derived EKE data are computed at the ocean surface only based on geostrophic velocity anomalies referenced to the 19 years altimetric period as follows:

$$EKE = \frac{1}{2}\left(u_G'^2 + v_G'^2\right)$$
$$u_G' = -\frac{g}{f}\frac{\partial \eta'}{\partial y}; \quad v_{IG} = \frac{g}{f}\frac{\partial \eta'}{\partial x} \tag{1}$$

where f is the Coriolis parameter, u'_G and v'_G are the zonal and meridional geostrophic velocities anomalies, and η' is the DT anomaly high-pass filtered as described in section 2.2. To compare both altimetric and modeled EKE at the surface, EKE is computed similarly to altimetry from the modeled SSH. In addition, to take advantage of the model synoptic velocity solution, EKE is also computed at each vertical levels of the

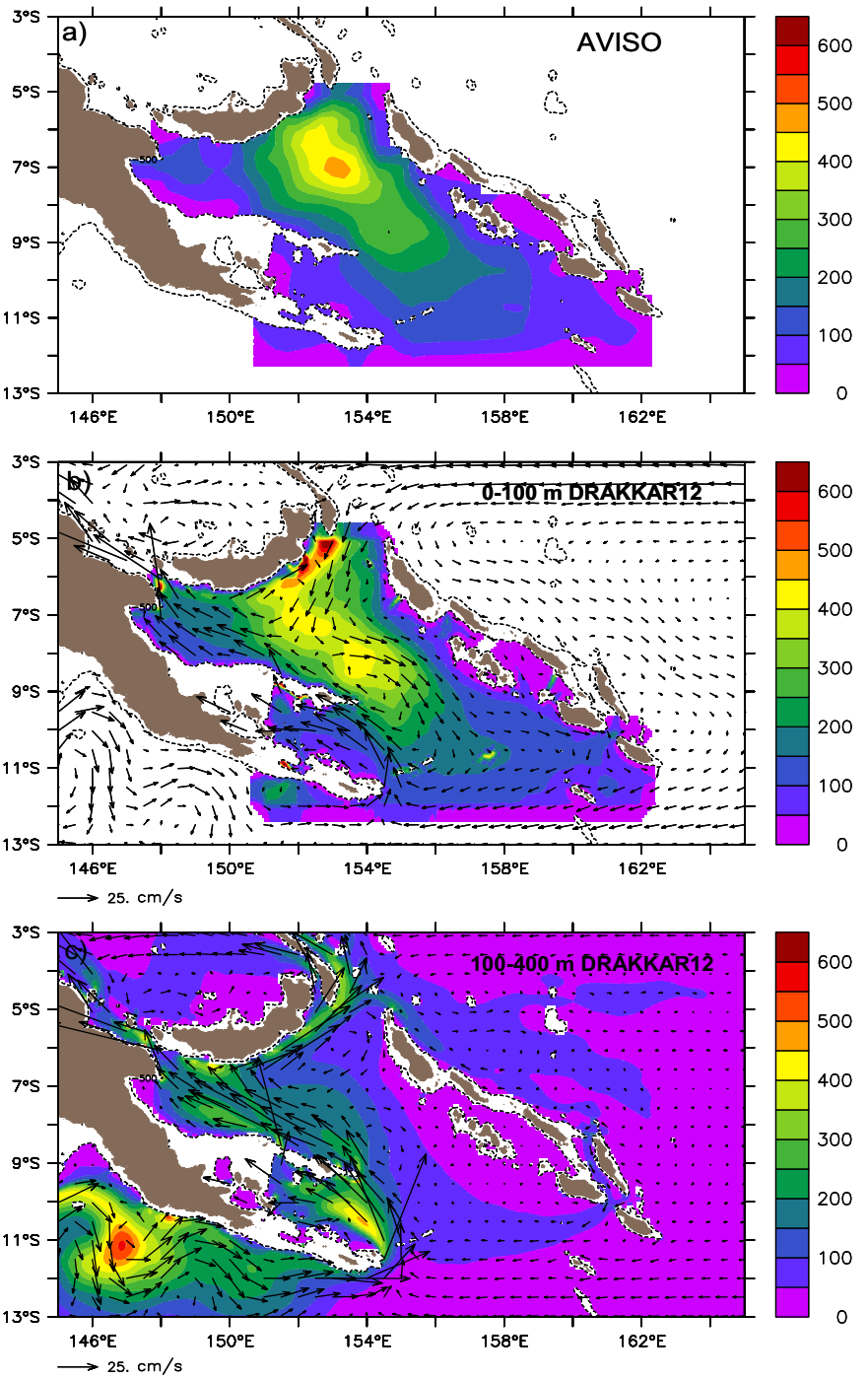

Figure 4. Mean EKE at the surface calculated from (a) the high-pass filtered gridded AVISO dynamic topography data and (b) the high-pass filtered SSH from the DRAKKAR12 simulation. The mean 0–100 m modeled surface circulation is superimposed (in cm/s, scale given at the bottom). (c) Mean 100–400 m modeled EKE (shading) and currents (arrows, in cm/s, scale given at the bottom). EKE unit is in cm^2/s^2.

model based on total velocity (not only their geostrophic component) anomalies relative to the 19 years model integration mean.

3.1. Mean Characteristics of the Mesoscale Variability

The LLWBCs (NGCU and NBCU) have their core at thermocline level [*Melet et al.*, 2010a; *Davis et al.*, 2012]. Therefore, the interaction of the LLWBCs with the bathymetry is expected to be the most effective in the thermocline range. Indeed, the EKE in this depth range seems to be generated by topographic effects at

the eastern extremities of PNG (e.g., Rossel Island and the Woodlark Archipelago), and extends equatorward following the western edge of the LLWBC pathways (Figure 4). Because the variability of the LLWBCs is rather limited compared with the circulation in the surface layers [*Davis et al*., 2012; *Melet et al*., 2013], the turbulence is quite stationary at thermocline level (not shown).

In the following, we focus on the EKE signal observed at the surface. The mean surface EKE distributions given by the model and altimetric data are consistent even though finer structures of EKE can be noticed in the model-derived EKE because of its higher resolution (Figure 4). Moreover, some local differences exist between the two surface EKE fields. For instance, a high EKE signal is simulated along the southern coast of the New Britain Island but is not present in the altimetric data. It is known that standard altimetric products are not reliable near coasts because near-coastal data are often removed during quality control checks. All in all, the mean surface EKE distributions from the model and altimetry are generally in a good enough agreement for the model to provide helpful complementary synoptic information to interpret the observed mesoscale variability from altimetry.

The mean surface EKE extends along the central Solomon Sea, reflecting the spatial distribution of high-frequency DT variability (Figure 3). The highest EKE levels (up to 400 cm^2/s^2) are located in the northern Solomon Sea. The latitude of the Woodlark Archipelago (9°S), where the Solomon Sea is narrower, seems to separate two regions different by their circulation characteristics as shown below. The superimposition of the 19 years mean simulated circulation averaged over 0–100 m depth on the simulated surface EKE field provides some evidence for the EKE distribution to be partly explained by the circulation mean patterns (Figure 4b). Surprisingly, high EKE levels seem to be more related to the SSI than to the strong NGCC. In the model, the highest levels of EKE are found at the mouth of Solomon Strait along the NB coast where the SSI overlays the opposite-flowing NBCU. As a result, the mean distribution of EKE at depth and at the surface is very different.

The high level of EKE observed in the Solomon Sea appears to be generated mainly by instabilities of the regional circulations since barotropic/baroclinic instabilities are the main mechanisms for eddy generation in most parts of the global ocean. In the following, we suggest that conditions are suitable for the development of instabilities due to vertical and horizontal shears as well as due to topographic effects. A measure of the potentiality for baroclinic instabilities to develop is given by the baroclinic time scale parameter (Tbc) which establishes the temporal scale for the growth of baroclinic waves [*Eady*, 1949]:

$$Tbc = \frac{Ri^{1/2}}{f}; \text{and } Ri = \frac{N^2}{|\frac{\partial U}{\partial z}|} \tag{2}$$

where f is the Coriolis parameter, Ri is the Richardson number where $|\frac{\partial U}{\partial z}|$ represents the vertical shear of the mean flow, and N is the mean stratification.

The shorter the baroclinic time scale parameter is, the faster baroclinic instabilities may develop. In the Solomon Sea, the short (0–10 days) 0–100 m depth averaged baroclinic time scale parameter clearly match regions where high EKE levels are found in the surface layers (Figure 5). The shortest baroclinic time scale (0–5 days) are associated with the high EKE level at depth that is related to the LLWBCs (e.g., the description above). There is also a close relationship with the surface EKE. For instance, the patch of high EKE simulated south of the New Britain island extends from the surface down to the core of the NBCU around 200 m depth (Figure 5c). The NBCU exhibits strong vertical shears enhanced in the surface layers by the SSI flowing in the opposite direction. The vertical shear between these two flows could be suitable for Kelvin-Helmholtz instabilities, and the tilt of the density surfaces could turn the current baroclinically unstable. More to the south, high EKE levels at 8°S are also associated with strong horizontal (at 230 m depth) and vertical (at 80 m depth) shears of the NGCU (at 151°E) (Figure 5b). At the surface, the highest level of EKE at 8°S extends down to 80 m depth, and is associated with the modulation of the SSI, as shown in section 3.2.

3.2. Time Modulation of the Mesoscale Variability

The time series of surface EKE averaged over the Solomon Sea exhibits low-frequency modulations at both seasonal and interannual time scales, and of similar magnitudes (Figure 6). It is true both for altimetry and

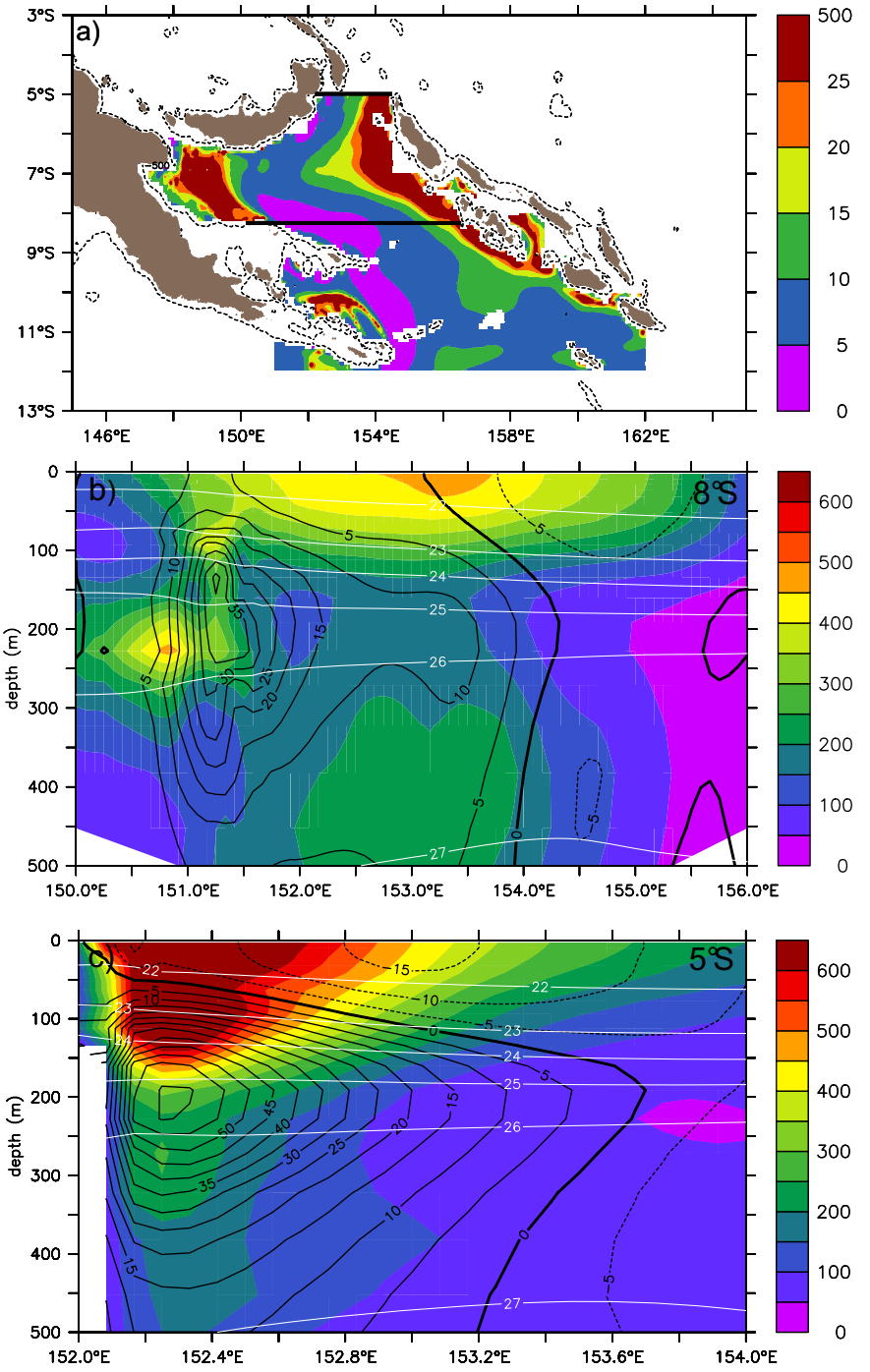

Figure 5. (a) Baroclinic time scale averaged over the 0–100 m surface layer (unit in days). The black lines indicate the location of the section presented below. Two longitude/depth sections at (b) 8°S and (c) 5°S (Solomon Strait) of the modeled EKE (shading, unit in cm^2/s^2), the mean current (contour, unit in cm/s), and of sigma theta (white isolines, unit in kg m^{-3}).

for the model, and the two time series are significantly phased ($r = 0.71$). Therefore, we can use either data set to discuss the seasonal cycle of the surface EKE or its low-frequency modulation.

3.2.1. Seasonal Modulation

The seasonal circulation in the Solomon Sea has been described using both in situ [*Cravatte et al.*, 2011; *Hristova and Kessler*, 2012] and satellite [*Melet et al.*, 2010b] data, and a model simulation [*Melet et al.*,

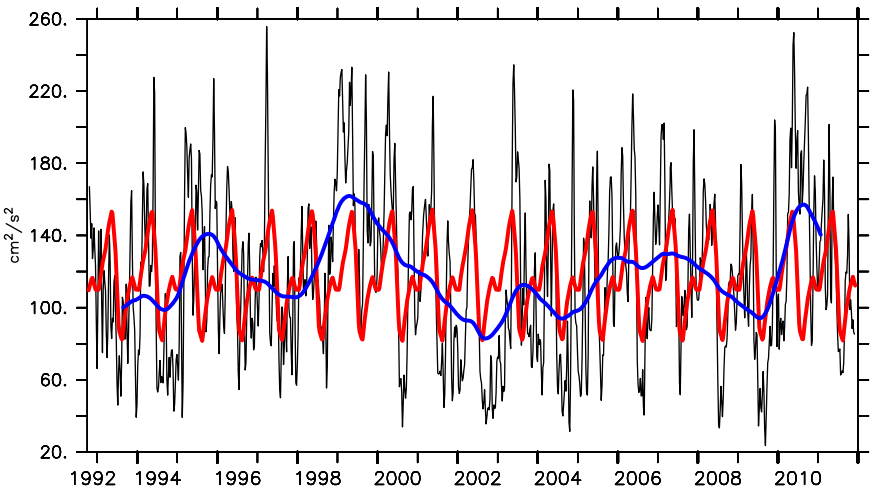

Figure 6. Time series of the Solomon Sea averaged raw EKE (black line), of its seasonal cycle (red line) and of its low-frequency modulation (blue line, half power at 18 months). EKE is calculated from the AVISO data and units are in cm^2/s^2.

2010a]. Results from these studies are consistent showing that the seasonal variability of the circulation is largely geostrophic in response to the basin-wide wind forcing that modulates incoming (GPC, NVJ, and SSI) and outgoing (NGCU-NGCC and NBCU) transports. The phasing of the annual cycle of the circulation results from the combination of different dynamical forcings. The annual march of the trade winds produces equatorial waves that control EUC variability and therefore the drawing of off-equatorial water during its austral spring-summer surge [*Yu and McPhaden*, 1999]. Off the equator and north of 10°S, annual wind stress curl variations propagating westward excite Rossby waves in the Central Pacific that are resonantly enhanced during their westward propagation [*Chen and Qiu*, 2004] and control the SEC inflow arriving at the eastern boundary of the Solomon Sea. Downwelling and upwelling Rossby waves arrive successively at latitudes spanning the Solomon Islands-New Ireland. These Rossby waves induce geostrophic velocity anomalies, and the background westward thermocline transport is enhanced from March (3°S) to October (10°S), whereas it is minimum from July (3°S) to April (10°S). South of 10°S, the annual march of the South Pacific Convergence Zone (SPCZ) induces a large wind stress variability in the subtropical South Pacific that generates a stationary, in-phase Rossby solution in the western subtropics [*Chen and Qiu*, 2004; *Kessler and Gourdeau*, 2007]. It results in a spin up (in austral spring) and down (in austral fall) of the western subtropical gyre. As a consequence, the northern branch of the gyre exhibits westward anomalies in austral spring, with a corresponding increase of the westward NVJ and a decrease of the eastward GPC. Although the interior ocean forcing presents a fairly simple pattern as described above, the response of the Solomon Sea circulation is more intricate because of the shape of the coast and of the lags introduced by the different forcing, as was analyzed by *Melet et al.* [2010a] for the thermocline circulation.

The seasonal cycle of the surface EKE is in phase over most of the Solomon Sea despite the difference in the mean surface EKE distribution between the northern and the southern basins. The magnitude of the annual cycle of the surface EKE averaged over the different basins is similar even if the mean EKE level is higher for the northern basin (Figure 7a). The EKE is maximum in May–June and minimum in September–February. A secondary peak is also visible in the northern basin in November, and the highest level of EKE along NB (north of 6.5°S) exhibits a seasonal cycle more spread and lagged by 1 month (maximum in July) compared with the rest of the basin. Therefore, EKE increases during the first half of the year, particularly after February. This corresponds to the month when the SSI increases drastically. The sharp EKE decrease during the June–September period corresponds to the increase of the NVJ which feeds the Solomon Sea through its southern open boundary. The relatively low level of EKE from October to January corresponds with a relatively low circulation in the Solomon Sea. During this period, both the SSI and the NVJ inflow are at their annual low values (Figure 7b). The secondary peak of EKE in November in the northern basin corresponds to an increase of the SSI in October (Figure 7b). This additional inflow does not extend to the far south, instead recirculating in the northern basin (not shown). Therefore, the seasonal variations of the surface EKE appear to be mostly sensitive to the intrusion of the SSI. An example is shown along the section at

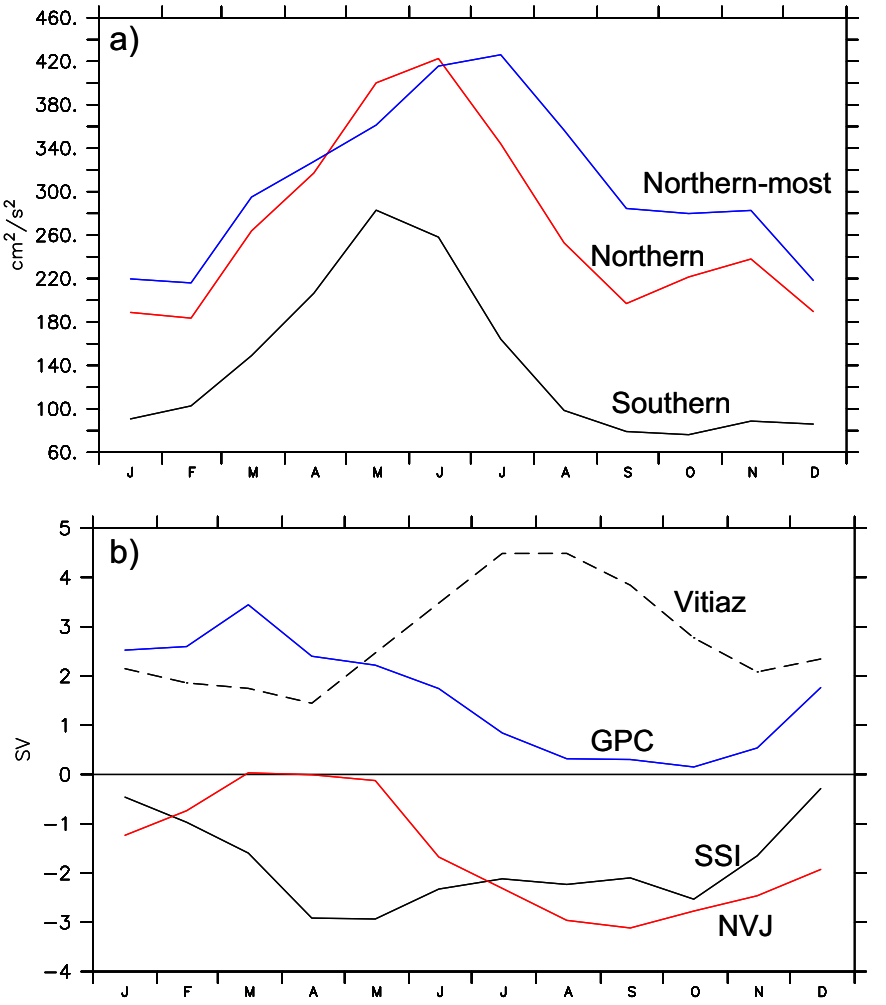

Figure 7. Seasonal cycle of (a) the surface EKE averaged over the southern Solomon Sea (defined as 11°S–9°S, black line), the northern Solomon Sea (defined as 9°S–5°S, red line) and the northern-most Solomon Sea (defined as 7°S–5°S, blue line). (b) Transports in the surface layer (0–100 m) of the different Solomon Sea inflows: the NVJ (defined at 162°E between 13°S and 11°S, red line), the GPC (defined at 148°E between 12°S and 10°S, blue line), and the SSI (defined as the southward current flowing through Solomon Strait at 5°S, black line); and of the outflow at Vitiaz Strait (dashed line). Unit is in Sv. Transports are positive for northward/westward currents.

8°S where the surface EKE is strongly associated with the maximum SSI in May (Figure 8). SSI appears to modulate both the vertical and horizontal shears allowing mixed barotropic/baroclinic instabilities to occur, which will be the subject of a dedicated study.

3.2.2. Low-Frequency Modulation

The Solomon Sea circulation exhibits a complex interannual variability related to the large-scale ENSO forcing. This low-frequency variability is mostly confined in the surface layer and the upper thermocline [*Melet et al.*, 2013]. At first order, the LLWBC transports in the Solomon Sea strengthen during El Niño conditions and weaken during La Niña conditions in order to counterbalance the interior geostrophic flow variability. Nevertheless, this simple large-scale picture is complicated because of the intricate bathymetry of the Solomon Sea. In particular, the narrowness of Vitiaz Strait actively constrains the outflowing transport through there. An asymmetry of the Solomon Sea circulation exists between El Niño and La Niña conditions. During El Niño conditions, the strengthening of the LLWBCs extends up to the surface and the bathymetric constraint at Vitiaz Strait is particularly effective by diverting more NGCU water into the NBCU and reducing the SSI. During La Niña conditions, the bathymetric constraint at Vitiaz Strait is less effective. The SSI is strengthened and a strong additional inflow occurs through Solomon Strait surface layers.

While EKE is mostly in phase over the Solomon Sea at annual time scales, low-frequency modulation of the surface EKE varies from one basin to the other (Figure 9a). Both EKE calculated from the altimetric DT

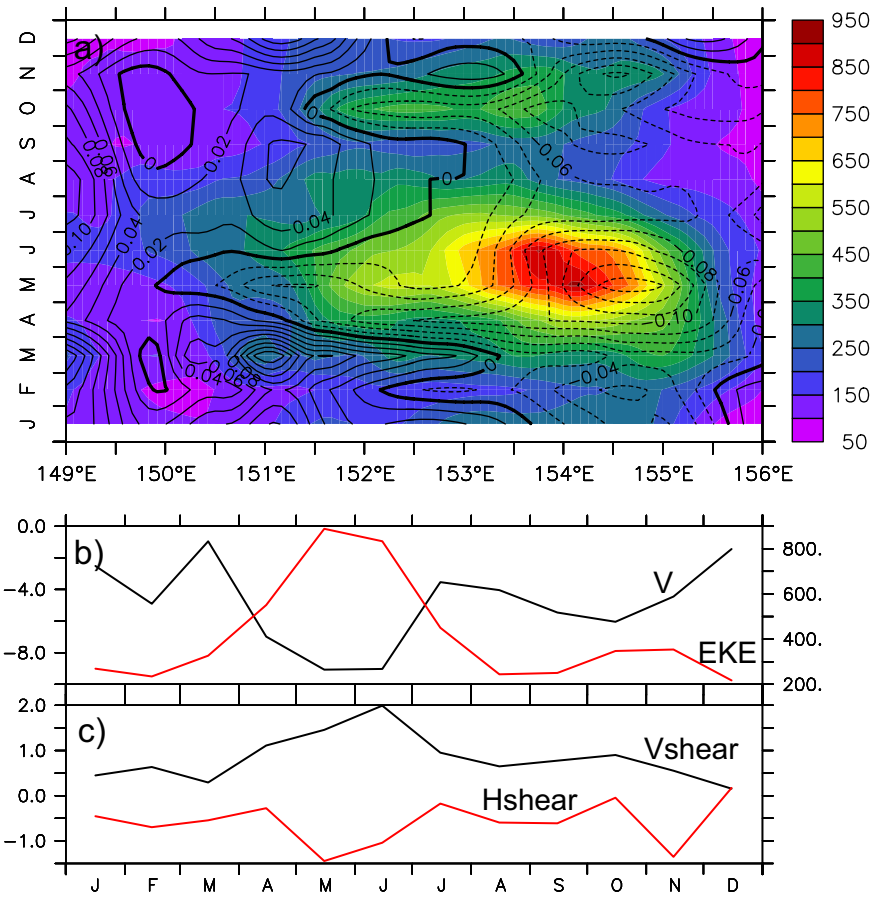

Figure 8. (a) Time/longitude section at 8°S across the Solomon Sea of the surface EKE (shading, in cm^2/s^2), and of the meridional current at the surface (contours, in m/s). (b) Seasonal cycle of the surface EKE (red line, in cm^2/s^2, right axis) and of the meridional current (black line, in cm/s, left axis) at 8°S–154°E (the longitude of the maximum EKE at 8°S). (c) Seasonal cycle of the horizontal (red, in $10^6\ s^{-1}$) and vertical (black, in $10^3\ s^{-1}$) shears of the meridional current in the surface layer (0–100 m).

and modeled SSH show similar out of phase EKE variations (not shown). The southern basin is closely linked to ENSO (correlation with the SOI of 0.76 and 0.79 for DT and SSH, respectively), whereas the northern basin is poorly correlated with ENSO (0.32 and 0.30 for DT and SSH, respectively), with a correlation as low as −0.07/−0.25 (for DT and SSH, respectively) for the far north part. In the southern basin, counterintuitively the surface EKE decreases during El Niño events when the NVJ and the LLWBCs are stronger (Figure 9b). In fact, it is associated with a decrease of the SSI. The opposite situation prevails during La Niña condition where the level of EKE is enhanced. This illustrates again the role of the SSI in the mesoscale activity of the Solomon Sea. This scenario is valid as far north as 7°S. In the far north basin, however the modulation of EKE consists of sporadic peaks (Figure 9c). These peaks correspond with a strong increase of the surface outflow at Vitiaz Strait during the 1991–1992 and 1997–1998 El Niño. These dates seem favorable for the bathymetric constraint at Vitiaz Strait to actively operate with the effect to increase the NBCU that extends up to the surface against the SSI that reverses at those dates (Figure 9b). EKE modulation between the south basin and the far north Solomon Sea is a complex mix of the different variability described above and no straightforward evidence exists to explain it.

4. Eddies in the Solomon Sea

In this section, "eddy" refers to a coherent mesoscale vortex dominated by nonlinear effects (i.e., the ratio of a particle velocity to the translation speed exceeds 1). The nonlinearity of the eddy implies that water can be trapped inside an eddy and be advected with it. Therefore, contrary to linear waves, eddies transport mass and properties such as heat, salt, and chemical tracers. Mesoscale activity detected by altimetry is not

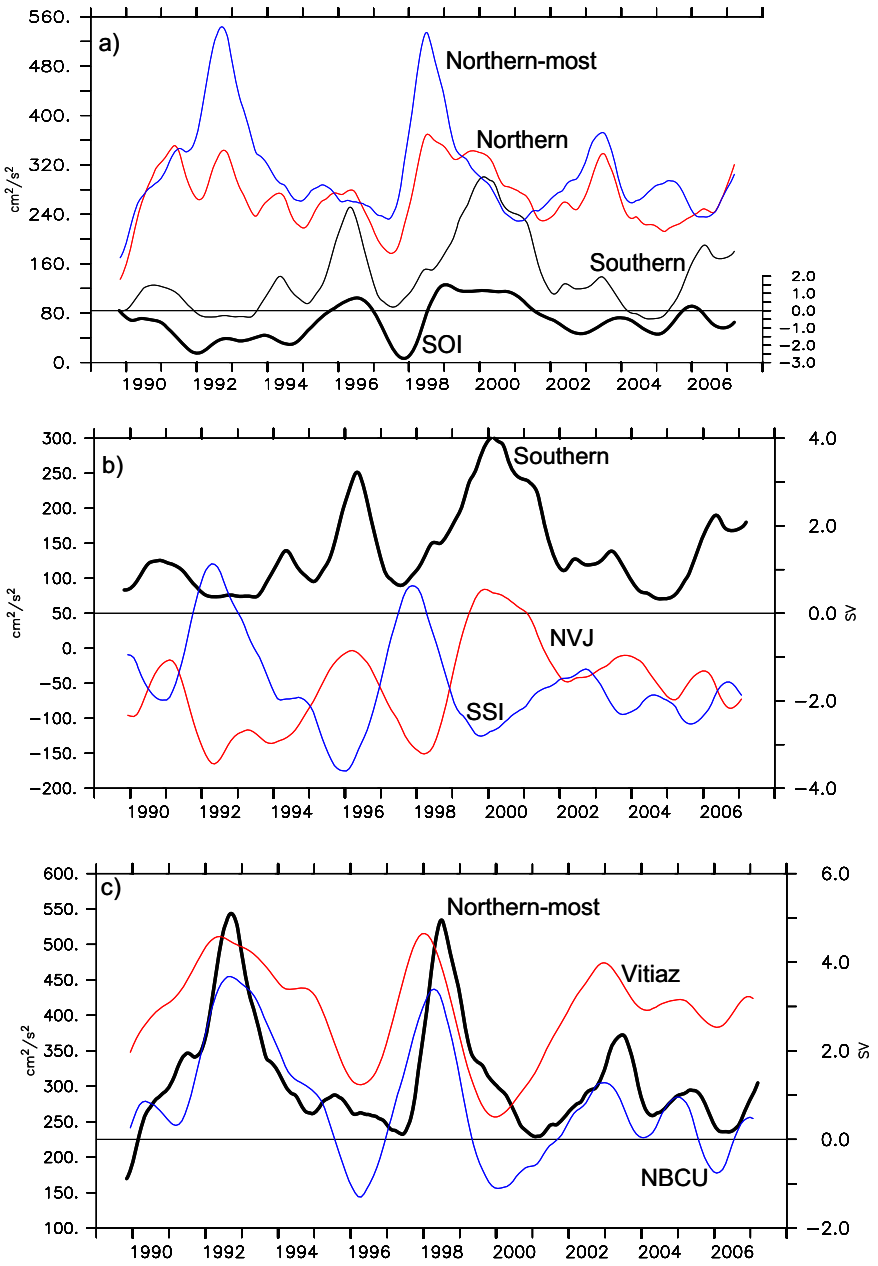

Figure 9. (a) Low-frequency modulation of the surface EKE averaged over the southern basin (black thin line), the northern basin (red line), and the northern-most Solomon Sea (blue line). Units in cm^2/s^2, left *y* axis. The thick black line represents the low-frequency modulation of the SOI (right *y* axis). (b) Low-frequency modulation of the surface EKE averaged over the southern basin (black line, in cm^2/s^2, left *y* axis), and of the 0–100 m depth transports from the NVJ (red line) and SSI (blue line). Transports are given in Sv (right *y* axis). (c) Low-frequency modulation of the surface EKE averaged over the northernmost basin (black line, in cm^2/s^2, left *y* axis), and of the 0–100 m depth transports from the NBCU (defined as the eastward current at 152°E extending 1° offshore NB, blue line) and of the Vitiaz outflow (red line). Transports are given in Sv (right *y* axis).

solely associated with the previously defined eddies. For instance, meanders of unstable currents also contribute to the mesoscale altimetric signal, and in a small basin like the Solomon Sea, mesoscale is not necessary associated with high frequency but also with mean structures and low frequency (see section 2.2). An examination of sequential maps of the raw DT fields clearly shows that coherent vortices are present in the Solomon Sea. In this section, a deterministic description of the cyclonic and anticyclonic eddies (respectively, referred to as CEs and AEs hereafter) in the Solomon Sea is provided, and we discuss the possible existence of both high- frequency and low-frequency mesoscale eddies.

4.1. Eddy Detection

Mesoscale coherent vortices are automatically detected in the altimetric DT maps and modeled SSH fields (the original data set without any filtering) using the winding-angle method developed by *Chaigneau et al*. [2009]. These identification and tracking algorithms have been used successfully in regional studies [*Wang et al*., 2003; *Nan et al*., 2011; *Chen et al*., 2011, 2012] and the efficiency of the winding-angle methods is discussed in *Souza et al*. [2011], *Kurian et al*. [2011], and *Nenciolli et al*. [2010]. To detect CE (AE), the algorithm first searches for potential eddy centers by locating local minima (maxima) of the DT/SSH fields in a moving window of $1^\circ \times 1^\circ$. Then, for each potential center, the algorithm looks for closed SLA contours with an increment of 10^{-3} m. The outermost closed contour embedding only one particular eddy center defines the edge of the eddy. Only eddies having a DT/SSH signature stronger than 2 cm are considered. For each identified eddy, the apparent radius (R) corresponds to the radius of an equivalent circular vortex having the same area, and the eddy energy (EE) corresponds to the mean EKE over the vortex. In a second step, each eddy is tracked from its appearance to its dissipation. Eddy tracking from one frame to the next one is performed by comparing each eddy of the current time frame with the ones located within a radius of 150 km in the next time frame. For each eddy pair having the same polarity, a cost function depending on the mismatch between their distance, vorticities, kinetic energies, and radii is evaluated. The corresponding eddy in the next time frame is then identified from the minimum of the cost function. Eddy trajectories and the evolution of their characteristics can therefore be identified.

Applying the eddy detection and tracking algorithms to the altimetric DT or to the modeled SSH fields provides similar results (not shown). We prefer to use the observational data set, i.e., the altimetric DT fields, to present the results. The eddy-tracking results show that no vortices originating from the open ocean propagate freely in the Solomon Sea, even through the southern boundary (not shown). Furthermore, no clear evidence was found of eddies generated east of the Solomon Sea [*Qiu and Chen*, 2004] squeezing through the gaps of the Solomon Islands. Thus, it appears that the great majority of eddies in the Solomon Sea are generated and stay inside this sea. It corroborates the geographical distribution of the EKE signal spreading along the central Solomon Sea. Eddies that were only identified once are discarded. A total of 2000 CEs and 1126 AEs were identified. In order to quantify and track robust features, only long-lived eddies ($>$3 weeks) are considered. They represent 1352 CEs and 581 AEs which correspond to 290 cyclonic eddies tracks and 174 anticyclonic eddies tracks. The role of the mean DT to explain the more numerous CEs compared to AEs is discussed below in section 4.3.

4.2. Characteristics

The characteristics of Solomon Sea mesoscale eddies are based on histograms of their radius, amplitude, energy, distance traveled (the distance between the initial and final locations), and lifespan, and some are presented in Figure 10. Both CEs and AEs have similar distribution of their radius with more than 55% of eddies having a radius between 80 and 120 km (not shown). Only 28% of AEs have a radius larger than 140 km against 44% for CEs. Regarding the amplitude of eddies, about 65% of eddies of them have an amplitude lower than 6 cm. CEs tend to have large amplitudes with more CEs than AEs having an amplitude higher than 8 cm (not shown). As a result, the EKE level for CEs is spread over a higher range of energy than for AEs (Figure 10a). The distances traveled by eddies are highly variable from relatively stationary eddies (30% of CEs and 20% of AEs have traveled less than 50 km) to eddies propagating over more than 600 km. CEs traveled over longer distances with 25% of CEs propagating over more than 300 km against 7% only for AEs. Moreover, lifespans of CEs are spread over longer-lived time than for AEs. To summarize, CEs are more energetic than AEs in the Solomon Sea, and their characteristics are more variable than that of AEs. A significant fraction of CEs is able to propagate over long distance whereas another significant fraction is rather stationary. This implies that AEs and CEs have different histories as shown below.

4.3. Spatial Distribution

The spatial occurrence of eddies looks like the spatial distribution of EKE with eddies mainly spreading along the central Solomon Sea, and particularly in the northern basin (Figure 11a). Furthermore, eddies are found in the south basin offshore of the Solomon Islands chain. The spatial distribution of CEs and AEs is different (Figures 11b and 11c). CEs dominate in the central Solomon Sea, particularly in the northern basin, and the maximum of occurrence are located in the two mesoscale cyclonic structures appearing in the mean circulation and mean SSH fields (e.g., Figure 1b). In fact, these mean cyclonic structures generate, but also trap

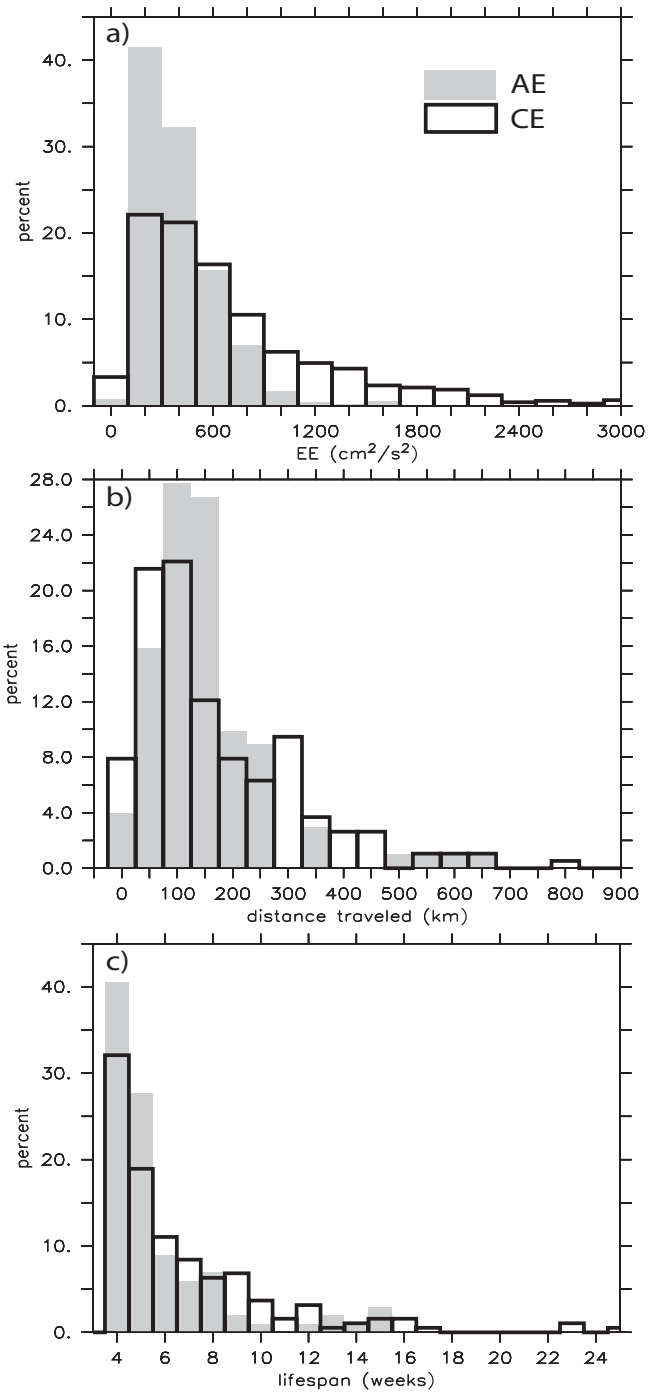

Figure 10. Histograms of the (a) energy, (b) traveled distance, and (c) lifespan of the Solomon Sea mesoscale eddies. The distributions are given for both the cyclonic (unfilled histogram) and anticyclonic eddies (filled histogram) as percentages of the total number of eddies.

eddies. This point is illustrated in Figures 12a and 12b where trajectories of stationary CEs (defined by a traveled distance shorter than 150 km and a lifespan longer than 2 months) are distinguished from that of propagating CEs (defined by a traveled distance longer than 300 km). Propagating CEs are mainly generated in a large band of latitudes between 8°S and 12°S, at the bounds between the northward LLWBC and the southward currents due to the SEC inflow through Solomon Strait (e.g., Figure 1b). They propagate to the northwest, probably advected by the LLWBC, and they are trapped in the mean northern cyclonic circulation where they dissipate (Figure 12b). Stationary CEs are part of the circulation in the northern Solomon Sea, which is characterized by cyclonic recirculations (section 2.2). The presence of such mean structures modulated at low frequency explains partly the higher number of CEs that are detected by comparison with AEs. As for the AEs, they are generated in two distinct areas of the eastern Solomon Sea. The first is located between 7°S and 8°S and the second one between 9°S and 10°S (with a large number of eddies generated along the coast, Figure 11c). They seem linked with the eastern edge of the SSI (see Figure 4b). The northern AE generation region corresponds to the location where a branch of the SSI turns eastward after encountering the LLWBC, whereas the southern AE generation region is located where this southeastward current encounters the Solomon Island coasts as shown by the mean surface circulation (Figure 1b). They preferentially propagate westward until they reach the LLWBC where they are no longer tracked (Figure 12c). They are probably dissipated as ocean western boundaries are not only the major eddy source areas but also the places where much of the eddy energy dissipates [*Zhai et al.*, 2010; *Xu et al.*, 2011]. The AE trajectories show that they can advect water masses from the SSI into the LLWBC, especially in the southeastern Solomon Sea. Since the water masses advected in the SEC and in the LLWBC have rather different thermodynamical characteristics because they originate from different latitudes, AEs could

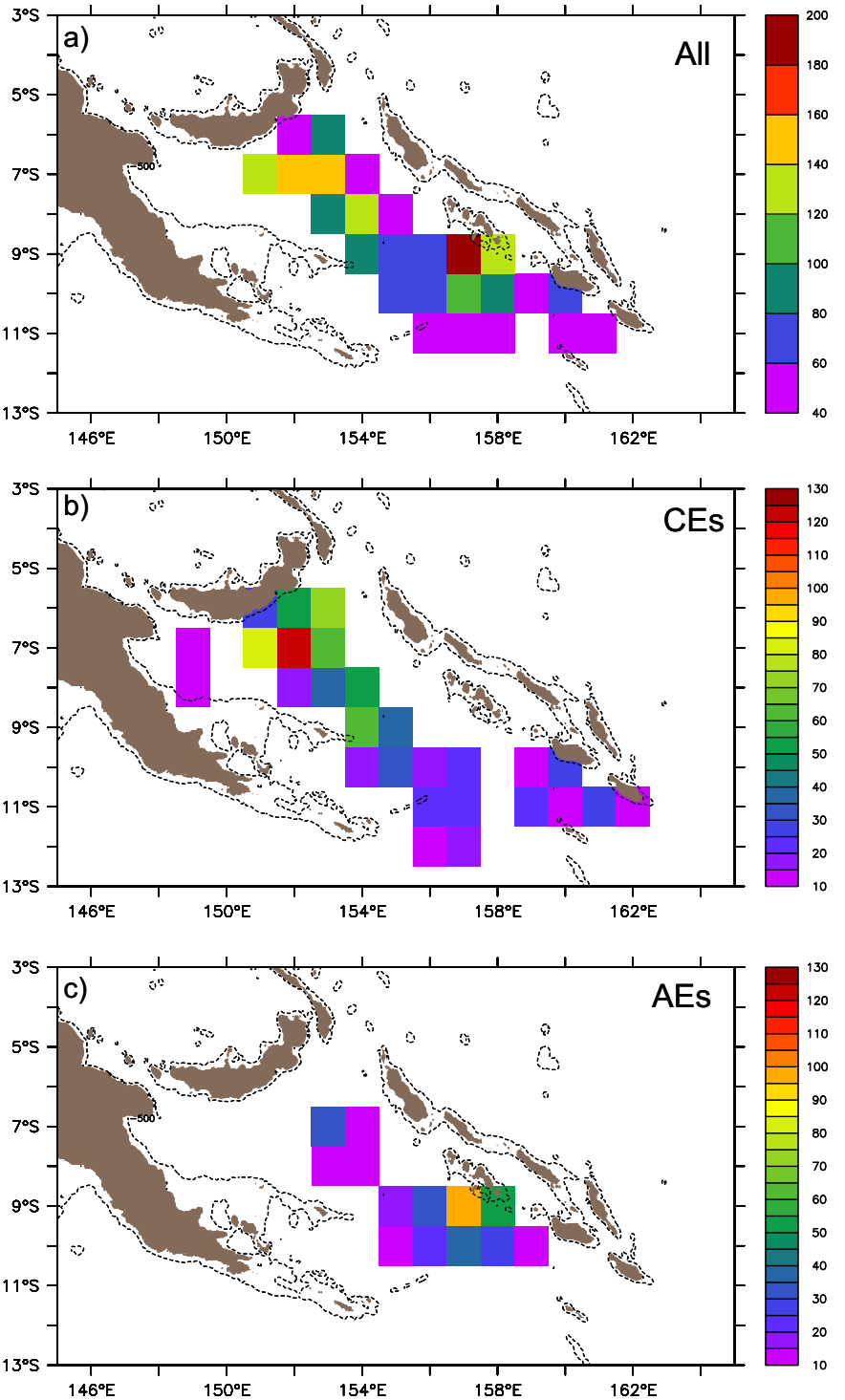

Figure 11. Spatial occurrence in the Solomon Sea during the 1993–2011 AVISO period of (a) all the eddies, (b) CEs, and (c) AEs. Unit is the number of eddies per month.

contribute to the modification of the LLWBCs temperature and salinity. Even though AEs are smaller and less energetic than CEs, they could play an important role in Solomon Sea water mass modification.

4.4. Variability

The signature of mesoscale eddies in the EKE signal is investigated in this section. Since long-lived CEs (>6 weeks) with a short traveled distance (<200 km) could be the result of a low-frequency modulation of the

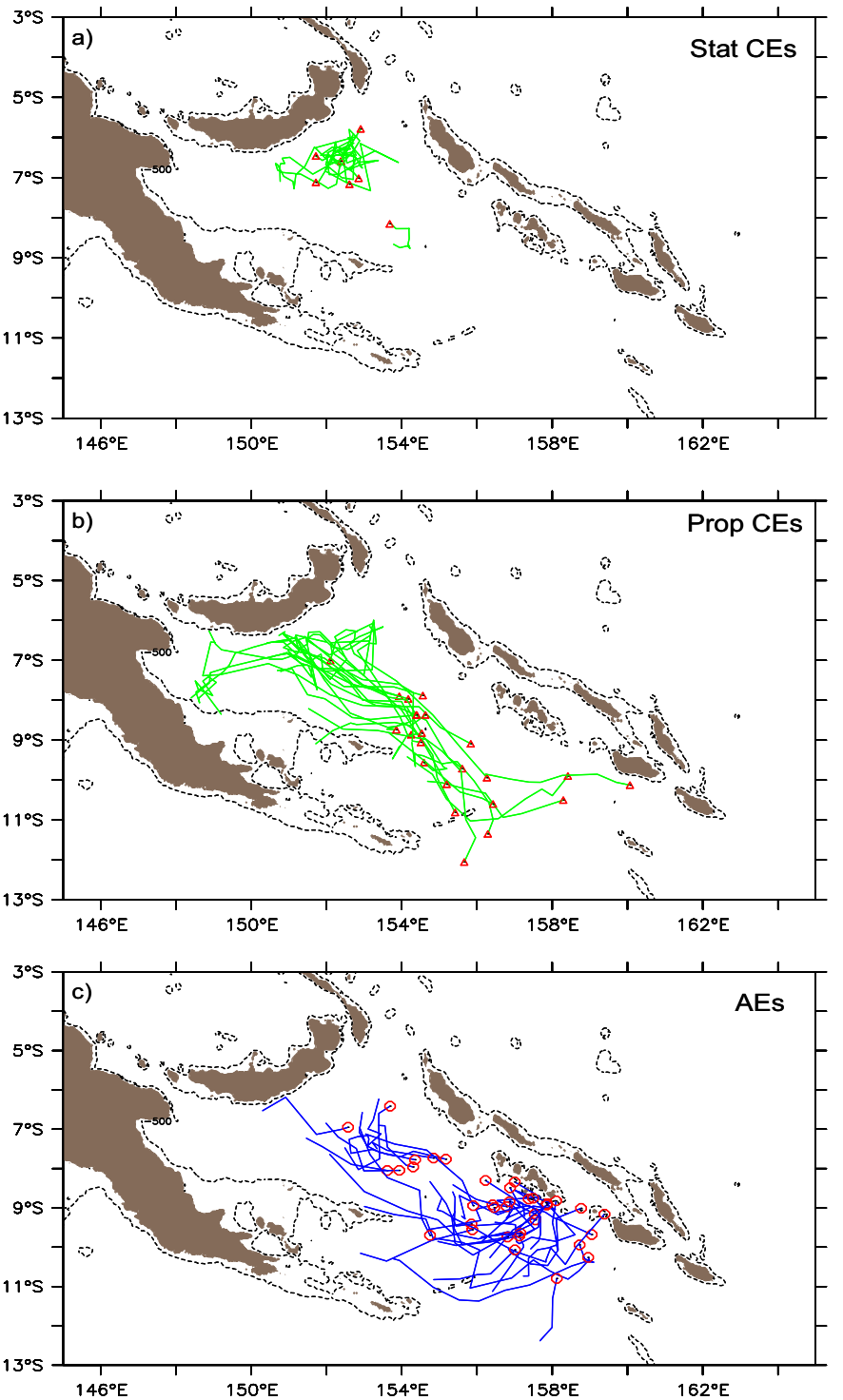

Figure 12. Trajectories of eddies tracked from altimetry with a long lifespan (>2 months) or a long distance traveled (>300 km): (a) stationary CEs, (b) propagating CEs, and (c) AEs. Symbols indicate the location where eddies were first detected.

regional circulation, they are not considered here. The time series of the surface EKE signal averaged over the Solomon Sea is similar to that of the number of the detected mesoscale eddies (Figure 13a, $r = 0.65$). Therefore, the modulation of the EKE in the Solomon Sea appears to be linked with the presence of coherent vortices. The EKE signal integrates the contribution of both AEs and CEs. Although CEs are more numerous and energetic than AEs, they do not clearly dominate the modulation of the EKE signal. Indeed, they

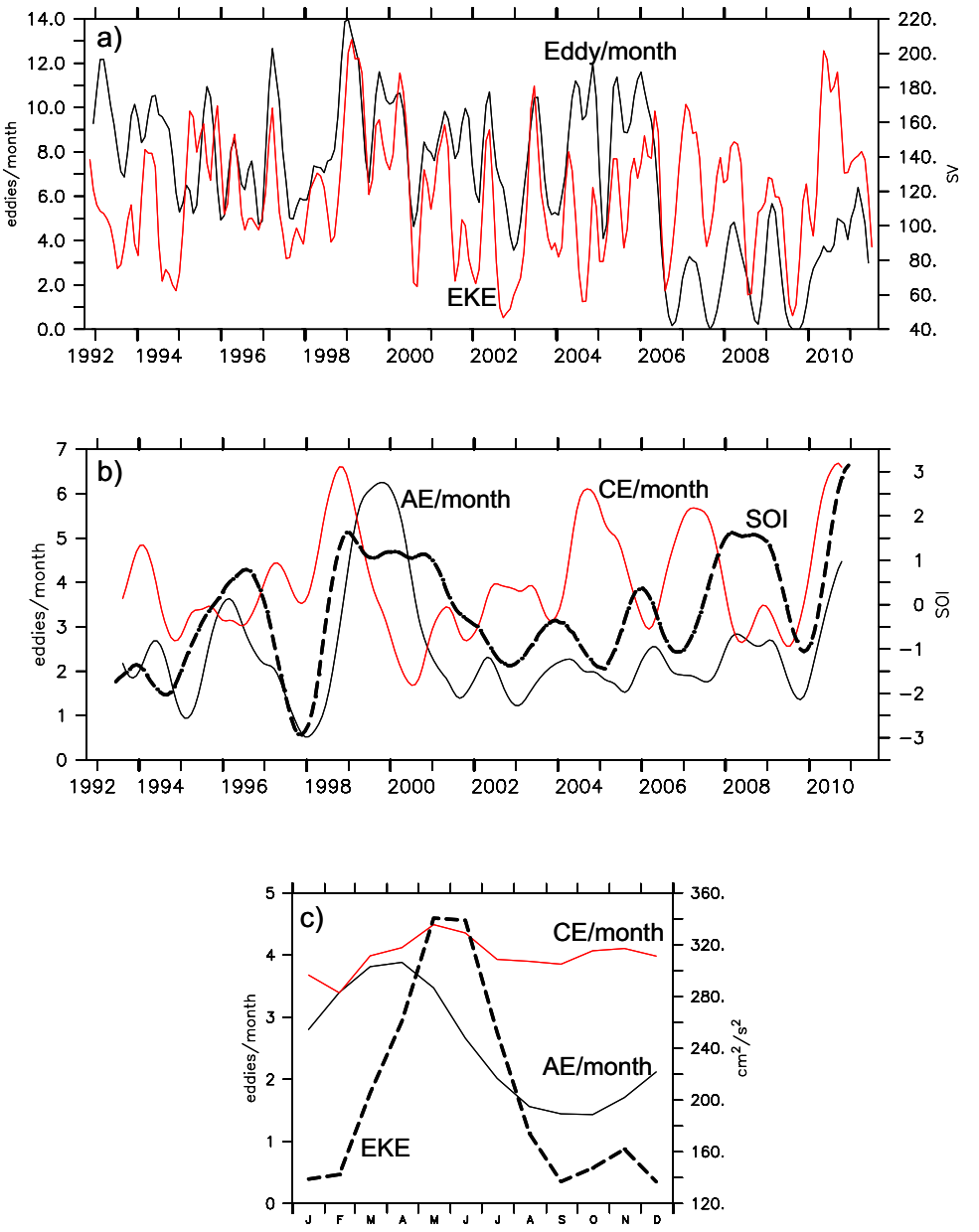

Figure 13. (a) Time series of the number of eddies per month (black line, left *y* axis) versus EKE (red line, right *y* axis, in cm^2/s^2). (b) Low-frequency evolution of the number per month of AEs (black line) and propagating CEs (red line, left *y* axis) versus the SOI (thick dashed line, right *y* axis). (c) Seasonal cycle of the number per month of AEs (black line) and propagating CEs (red line, left *y* axis) versus the Solomon Sea averaged surface EKE (thick dashed line, right *y* axis).

are poorly correlated to EKE ($r = 0.30$) whereas the time series of the number of AEs is well correlated with the EKE ($r = 0.65$). Therefore, both AEs and CEs have different histories, and both are important to explain the observed variability as shown below.

At seasonal time scales, the variability in the number of detected eddies is more well marked for AEs than for CEs. However, the annual cycle of EKE seems to be more consistent with the annual cycle of CEs (Figure 13c). This is in accordance with the spatial distribution of EKE in the central Solomon Sea that matches the spatial occurrence of CEs. The maximum number of AEs is reached in March–April, and its minimum in September–October. The maximum number of AEs corresponds with an increase of the SEC inflow and a decrease of the NVJ. The number of CEs is maximum 2 months later and coincides with the EKE maximum. Then, the decrease

of EKE follows the decrease of the mesoscale eddy activity and reaches a minimum in September. A secondary peak exists in the cycle of both CEs and EKE in November.

At interannual time scales, the link between the eddy activity in the Solomon Sea and ENSO is more obvious when the interannual variability of the number of AEs and CEs is examined separately (Figure 13b). In fact, AEs and CEs behave differently. The number of AEs is in phase with the SOI (correlation of 0.67). It increases during La Niña conditions and decreases during El Niño conditions. It is in accordance with the low-frequency modulation of EKE in the southern part of the basin described in section 3.2 with the EKE increasing during La Niña and decreasing during El Niño ($r = 0.81$). As for CEs, the link with the SOI is not obvious even though an increase of CEs seems to appear 6–8 months after an El Niño. This signature seems to be more in accordance with the low-frequency modulation of the EKE observed in the northern basin.

5. Summary

This study is an initial documentation of mesoscale activity in the Solomon Sea, using altimetric DT data and a high-resolution numerical model simulation. The Solomon Sea represents a transit area for the LLWBCs connecting the subtropics to the equatorial Pacific, which are thought to play a major role in ENSO evolution. It has been shown that the Solomon Sea circulation is complex with well-marked seasonal and interannual cycles, and a high level of eddy kinetic energy. However, the mesoscale dynamics has never been studied so far in spite of its potential impact on the circulation, transport, and mixing in this region. Since the Solomon Sea water masses ultimately reach the equatorial surface Pacific and could impact the basin-wide climate, it is important to know how these water masses are conditioned. At this stage, the objective is to provide a basic description of mean properties of Solomon Sea mesoscale variability for further investigation of its dynamics. In this paper, we examined the relation between the eddy kinetic energy (EKE) at the surface and mesoscale eddy activity, and how they are related to the seasonal/interannual variability of the main currents. Some insights on possible mechanisms at the origin of this mesoscale activity were identified.

In the open ocean, mesoscale dynamics usually refer to coherent vortices dominated by nonlinear effect with typical space and time scales of 50–500 km and 10–100 days. In a marginal sea like the Solomon Sea, this picture is complicated by a regional circulation exhibiting features at spatial mesoscale and low frequency. Indeed, two cyclonic structures, located in the northern basin and at the extremity of the Woodlark Archipelago, are present in the mean circulation of the Solomon Sea, and low-frequency mesoscale patches are also present in the northern basin and in the southeastern basin offshore Solomon Islands. It requires to take into account such features in our mesoscale analysis by suppressing them from the EKE signal and to distinguish between eddies associated with such structures from the others able to propagate freely.

Observed and modeled high-pass-filtered EKE are generally consistent in terms of magnitude and spatial patterns. However, some localized differences exist, such as the stronger EKE magnitude in the model along the New Britain coast that cannot be observed from standard altimetry. The highest EKE is observed in the northern part of the basin and extends diagonally southeastward into the central basin along the axis of the Solomon Sea. This spatial distribution of mean EKE is consistent with the spatial occurrence of eddies in the Solomon Sea. It means that the great majority of eddies in the Solomon Sea are generated and stay inside this sea.

An interesting point emerging from the analysis of observations and model outputs is that eddies are predominantly cyclonic, partly due to stationary and long life cyclonic eddies associated with the mesoscale structures present in the mean circulation. Propagating cyclonic eddies (CEs) are mainly generated in a large band of latitudes between 8°S and 12°S, at the bounds between the northward NGCC and the southward SSI (originating in the SEC intrusion at Solomon Strait). They propagate to the northwest probably advected by the LLWBC. As for anticyclonic eddies (AES), they are generated in the eastern part of the Solomon Sea and propagate westward until reaching the LLWBCs where they probably dissipate.

Both the EKE level and the eddy activity in the Solomon Sea are related to variations in the strength of the different currents entering the Solomon Sea, namely the GPC, the NVJ through the southern boundary and the SSI. In fact, mesoscale activity in the Solomon Sea is intimely linked to the highly variable SSI.

At seasonal cycle, the surface EKE increases with the number of AEs after February, and is maximum in May which coincides with the maximum number of CEs. This corresponds to the period when the SSI increases drastically. The sharp EKE decrease during the June–September period when the SSI slows down and the NVJ drastically increases. The relatively low level of EKE from October to January corresponds with low values of both the SSI and the NVJ inflow.

At ENSO time scale, the southern and northern basins, and the anticyclonic and cyclonic eddies behave differently. In the southern basin, the surface EKE surprisingly decreases during El Niño events when the NVJ and the LLWBCs are stronger. In fact, this EKE decrease is associated with a decrease of the SSI. The opposite situation prevails during La Niña condition where the level of EKE is enhanced in relation to the number of AEs. In the northern basin, the situation is more complex, and EKE appears to be also sensitive to the effect of the bathymetric constraint at Vitiaz Strait when it actively operates. This low-frequency modulation of the EKE seems to be in accordance with an increase of the number of CEs 6–8 months after an El Niño.

The mesoscale activity in the Solomon Sea appears to be generated mainly by instabilities of the regional circulations, and the SSI appears to modulate both the vertical and horizontal shears allowing mixed barotropic/baroclinic instabilities to occur. For instance, the vertical shear of the eastward NBCU, enhanced in the surface layers by the SSI flowing in the opposite direction, could be suitable for Kelvin-Helmholtz instabilities, and could turn the current baroclinically unstable. Regarding the northward NGCU, *Walker and Pedlosky* [2002] demontrate that meridional currents with such a vertical shear are baroclinically unstable. Also, the horizontal shear between the northward LLWBC and southward SSI could be suitable for barotropic instability as suggested by Figure 8. The type of instability that leads to the eddy growth in the Solomon Sea cannot be determined from the present analysis and will be the subject of a dedicated study.

Future work would involve an examination of the dynamical aspect of the Solomon Sea mesoscale activity, and of the nature of the instability mechanism by considering the energy transfer rates into the energy of the eddies from either the potential energy or the kinetic energy of the mean flow (Lorenz energy cycle) [e.g., *Lorenz*, 1955; *Storch et al*., 2012]. This approach could be completed by the analysis of glider data [*Davis et al*., 2012]. Glider monitoring of the Solomon Sea started as part of the Consortium on the Ocean's Role in Climate (CORC) program on boundary current in 2007. *Davis et al*. [2012] mention typical fluctuations of depth-averaged velocities of $O(10\ \mathrm{cm\ s^{-1}})$ with typical scales of 100–200 km in the eastern basin that might be due to waves or migrating eddies. The glider data could be used in conjunction with altimetry to detect the mesoscale structures crossed by the glider providing information on their vertical structure, and of their effective role in modifying water mass properties. Based on the actual limits of altimetry and of the model resolution here, the smaller scales that we are able to investigate in this study are about of 100 km. Therefore, a large part of the kinetic energy spectrum is missing. An effort has been made recently to develop 1/36° regional models of the Solomon Sea (B. Djath et al., Multiscale dynamical analysis of a high resolution numerical model simulation of the Solomon Sea circulation, submitted to *Journal of Geophysical Research: Oceans*, 2014; H. G. Hristova et al., Mesoscale variability in the Solomon Sea: Seasonal equilibrium simulation and characteristics with a nested ROMS model, submitted to *Journal of Geophysical Research: Oceans*, 2014). The meso and submesoscale activity in the Solomon Sea could soon be examined from the 1/36° simulations. Moreover, the new altimetric missions including SARAL-AltiKa (launched in February of 2013) and the future wide-swath SWOT mission are great opportunities to explore finer scales in this region of complex bathymetry and strong currents.

Acknowledgments

This work is a contribution to the CLIVAR/SPICE international program. This research has been conducted with the support of the Centre National d'Etudes Spatiales (CNES/TOSCA), the Centre National de la Recherche Scientifique (CNRS/INSU LEFE), and the Institut de Recherche pour le Développement (IRD). The authors would like to thank the DRAKKAR team for providing them with the high-resolution global ocean simulation, and especially J.M. Molines for his availability. We also thank A. Chaigneau for his help using the identification and tracking algorithms.

References

Adcroft, A., C. Hill, and J. Marshall (1997), Representation of topography by shaved cells in a height coordinate ocean model, *Mon. Weather Rev.*, *125*(9), 2293–2315.

Barnier, B., et al. (2006), Impact of partial steps and momentum advection schemes in a global ocean circulation model at eddy permitting resolution, *Ocean Dyn.*, *56*(5–6), 543–567.

Butt, J., and E. Lindstrom (1994), Currents off the east coast of New Ireland, Papua New Guinea, and their relevance to regional undercurrents in the western Equatorial Pacific Ocean, *J. Geophys. Res.*, *99*(C6), 12,503–12,514.

Carton, J. A., and Y. Chao (1999), Caribbean Sea eddies inferred from TOPEX/Poseidon altimetry and a 1/6° Atlantic ocean model circulation, *J. Geophys. Res.*, *104*(C4), 7743–7752.

Chaigneau, A., G. Eldin, and B. Dewitte (2009), Eddy activity in the four major upwelling systems from satellite altimetry (1992–2007), *Prog. Oceanogr.*, *83*, 117–123, doi:10.1016/j.pocean.2009.07.012.

Chelton, D. B., R. A. de Szoeke, M. G. Schlax, K. El Naggar, and N. Siwertz (1998), Geographical variability of the first-baroclinic Rossby radius of deformation, *J. Phys. Oceanogr.*, *28*, 433–460.

Chelton, D. B., M. G. Schlax, and R. M. Samelson (2011), Global observations of nonlinear mesoscale eddies, *Prog. Oceanogr.*, *91*, 167–216, doi:10.1016/j.pocean.2011.01.002.
Chen, G., Y. Hou, and X. Chu (2011), Mesoscale eddies in the South China Sea: Mean properties, spatiotemporal variability, and impact on thermohaline structure, *J. Geophys. Res.*, *116*, C06018, doi:10.1029/2010JC006716.
Chen, G., D. Wang, and Y. Hou (2012), The features and interannual variability mechanism of mesoscale eddies in the Bay of Bengal, *Cont. Shelf. Res.*, *47*, 178–185.
Chen, S., and B. Qiu (2004), Seasonal variability of the South Equatorial Countercurrent, *J. Geophys. Res.*, *109*, C08003, doi:10.1029/2003JC002243.
Cravatte, S., A. Ganachaud, Q. P. Duong, W. S. Kessler, G. Eldin, and P. Dutrieux (2011), Observed circulation in the Solomon Sea from SADCP data, *Prog. Oceanogr.*, *88*, 116–130.
Davis, R. E., W. S. Kessler, and J. T. Sherman (2012), Gliders measure western boundary current transport from the south Pacific to the equator, *J. Phys. Oceanogr.*, *42*, 2001–2013, doi:10.1175/JPO-D-12-022.1.
Donguy, J.-R. (1994), Surface and subsurface salinity in the tropical Pacific Ocean: Relations with climate, *Prog. Oceanogr.*, *34*, 45–78.
Eady, E. T. (1949), Long waves and cyclone waves, *Tellus*, *1*, 33–52.
Fu, L. (2009), Pattern and velocity of propagation of the global ocean eddy variability, *J. Geophys. Res.*, *114*, C11017, doi:10.1029/2009JC005349.
Ganachaud, A., et al. (2008), Southwest Pacific Ocean Circulation and Climate Experiment (SPICE). Part II: Implementation Plan, *NOAA OAR Spec. Rep., CLIVAR Publ. Ser. 133*, 36 pp., Int. CLIVAR Proj. Off., NOAA/OAR/PMEL, Seattle, Wash.
Ganachaud, A., et al. (2012), Naming a western boundary current from Australia to the Solomon Sea, *CLIVAR Exch. Newslett.*, *17*(1), 28.
Garrett, C., and E. Kunze (2007), Internal tide generation in the deep ocean, *Annu. Rev. Fluid Mech.*, *39*, 57–87.
Grenier, M., S. Cravatte, B. Blanke, C. Menkes, A. Koch-Larrouy, F. Durand, A. Melet, and C. Jeandel (2011), From the western boundary currents to the Pacific Equatorial Undercurrent: Modeled pathways and water mass evolutions, *J. Geophys. Res.*, *116*, C12044, doi:10.1029/2011JC007477.
Hristova, H., and W. S. Kessler (2012), Surface circulation in the Solomon Sea derived from Lagrangian drifter observations, *J. Phys. Oceanogr.*, *42*, 448–458.
Hwang, C., and S. A. Chen (2000), Circulations and eddies over the South China Sea derived from TOPEX/Poseidon altimetry, *J. Phys. Oceanogr.*, *105*(10), 23,943–23,965.
Jouanno, J., J. Sheinbaum, B. Barnier, and J. M. Molines (2009), The mesoscale variability in the Caribbean Sea. Part II: Energy sources, *Ocean Modell.*, *26*, 226–239, doi:10.1016/j.ocemod.2008.10.006.
Kessler, W. S., and L. Gourdeau (2007), The annual cycle of circulation of the southwest subtropical Pacific, analyzed in an ocean GCM, *J. Phys. Oceanogr.*, *37*, 1610–1627.
Kurian, J., F. Colas, X. Capet, J. C. McWilliams, and D. B. Chelton (2011), Eddy properties in the California Current System, *J. Geophys. Res.*, *116*, C08027, doi:10.1029/2010JC006895.
Large, W., and S. Yeager (2004), Diurnal to decadal global forcing for ocean and sea-ice models: The data sets and Flux climatologies, *Tech. Note NCAR/TN-460+STR*, CGD Div. of the Natl. Center for Atmos. Res., Boulder, Colo.
Large, W. G., and S. Yeager (2009), The global climatology of an interannually varying air-sea flux data set, *Clim. Dyn.*, *33*, 341–364, doi:10.1007/s00382-008-0441-3.
Lecointre, A., J. M. Molines, and B. Barnier (2011), Definition of the interannual experiment ORCA12.L46-MAL95, 1989–2007, internal report, MEOM-LEGI, CNRS, LEGI-DRA 21-10-2011, 25 pp., Grenoble, France.
Le Traon, P.-Y., and R. Morrow (2001), Ocean currents and eddies, in *Satellite Altimetry and Earth Sciences: A Handbook for Techniques and Applications*, edited by L.-L. Fu and A. Cazenave, pp. 171–210, Academic, San Diego, Calif.
Le Traon, P.-Y., P. Klein, B. L. Hua, and G. Dibarboure (2008), Do altimeter data agree with interior or surface quasigeostrophic theory?, *J. Phys. Oceanogr.*, *38*(5), 1137–1142.
Levitus, S., T. Boyer, M. Conkright, T. O. Brien, J. Antonov, C. Stephens, L. Stathoplos, D. Johnson, and R. Gelfeld (1998), *NOAA Atlas NESDIS 18, World Ocean Database 1998: Introduction*, vol. 1, 346 pp., U.S. Gov. Print. Off., Washington, D. C.
Lorenz, E. N. (1955), Available potential energy and the maintenance of the general circulation, *Tellus*, *7*(2), 157–167.
Luo, J., and T. Yamagata (2001), Long-term El Niño-Southern Oscillation (ENSO)-like variation with special emphasis on the South Pacific, *J. Geophys. Res.*, *106*, 22,211–22,227.
Luo, J.-J., S. Masson, S. Behara, P. Delecluse, S. Gualdi, A. Navarra, and T. Yamagata (2003), South Pacific origin of the decadal ENSO-like variation simulated by a coupled GCM, *Geophys. Res. Lett.*, *30*(24), 2250, doi:10.1029/2003GL018649.
Luo, Y., L. Rothstein, R. Zhang, and A. Busalacchi (2005), On the connection between South Pacific subtropical spiciness anomalies and decadal equatorial variability in an ocean general circulation model, *J. Geophys. Res.*, *110*, C10002, doi:10.1029/2004JC002655.
Madec, G. (2008), NEMO ocean engine, Tech. rep., Institut Pierre Simon Laplace (IPSL), France, 300 pp (Note du Pole de Modélisation, 27).
Marchesiello, P., X. Capet, C. Menkes, and S. C. Kennan (2011), Submesoscale dynamics in tropical instability waves, *Ocean Modell.*, *39*, 31–46.
Melet, A., L. Gourdeau, W. S. Kessler, J. Verron, and J. M. Molines (2010a), Thermocline circulation in the Solomon Sea: A modeling study, *J. Phys. Oceangr.*, *40*, 1302–1319.
Melet, A., L. Gourdeau, and J. Verron (2010b), Variability in Solomon Sea circulation derived from altimeter sea level data, *Ocean Dyn.*, *60*, 883–900.
Melet, A., J. Verron, L. Gourdeau, and A. Koch-Larrouy (2011), Equatorward pathways of Solomon Sea water masses and their modifications, *J. Phys. Oceanogr.*, *41*, 810–826, doi:10.1175/2010JPO4559.1.
Melet, A., L. Gourdeau, J. Verron, and B. Djath (2013), Solomon sea circulation and water mass modifications: Response at ENSO timescales, *Ocean Dyn.*, *63*(1), 1–19, doi:10.1007/s10236-012-0582-0.
Morrow, R. A., F. Birol, D. Griffin, and J. Sudre (2004), Divergent pathways of cyclonic and anti-cyclonic ocean eddies, *Geophys. Res. Lett.*, *31*, L24311, doi:10.1029/2004GL020974.
Nan, F., H. Xue, F. Chai, L. Shi, M. Shi, and P. Guo (2011), Identification of different types of Kuroshio intrusion into the South China Sea, *Ocean Dyn.*, *61*, 1291–1304, doi:10.1007/s10236-011 0426-3.
Nencioli, F., C. Dong, T. Dickey, L. Washburn, and J. McWilliams (2010), A vector geometry based eddy detection algorithm and its application to high-resolution numerical model products and high-frequency radar surface velocities in the Southern California Bight, *J. Atmos. Ocean Technol.*, *27*(3), 564–579, doi:10.11.1175/2009JTECHO725.1.
Niwa, Y., and T. Hibiya (2001), Numerical study of the spatial distribution of the M2 internal tide in the Pacific Ocean, *J. Geophys. Res.*, *106*, 22,441–22,449.

Nonaka, M., and H. Sasaki (2007), Formation mechanism for isopycnal temperature-salinity anomalies propagating from the eastern South Pacific to the equatorial region, *J. Clim.*, *20*, 1305–1315.
Pascual, A., Y. Faugère, G. Larnicol, and P.-Y. Le Traon (2006), Improved description of the ocean mesoscale variability by combining four satellite altimeters, *Geophys. Res. Lett.*, *33*, L02611, doi:10.1029/2005GL024633.
Pedlosky, J. (2000), The transparency of ocean barriers to Rossby waves: The Rossby slit problem, *J. Phys. Oceanogr.*, *31*, 336–352.
Penduff, T., J. Le Sommer, B. Barnier, A.-M. Tréguier, J.-M. Molines, and G. Madec (2007), Influence of numerical schemes on current-topography interactions in 1/4° global ocean simulations, *Ocean Sci.*, *3*, 509–524.
Qiu, B., and S. Chen (2004), Seasonal modulations in the eddy field of the South Pacific Ocean, *J. Phys. Oceanogr.*, *34*, 1515–1527.
Rio, M. H., S. Guinehut, and G. Larnicol (2011), New CNES-CLS09 global mean dynamic topography computed from the combination of GRACE data, altimetry, and in situ measurements, *J. Geophys. Res.*, *116*, C07018, doi:10.1029/2010JC006505.
Roemmich, D., and J. Gilson (2001), Eddy transport of heat and thermocline waters in the North Pacific: A key to interannual/decadal climate variability, *J. Phys. Oceanogr.*, *31*, 675–687.
Simmons, H. F., and D. Nof (2002), The squeezing of eddies through gaps, *J. Phys. Oceanogr.*, *32*, 314–335.
Souza, J. M. A., C. de Boyer Montégut, and P. Y. Le Traon (2011), Comparison between three implementations of automatic identification algorithms for the quantification and characterization of mesoscale eddies in the South Atlantic Ocean, *Ocean Sci. Discuss.*, *8*, 483–531, doi:10.5194/osd-8–483-2011.
Stammer, D. (1998), On eddy characteristics, eddy transports, and mean flow properties, *J. Phys. Oceanogr.*, *28*, 727–739.
Tsuchiya, M., R. Lukas, R. A. Fine, E. Firing, and E. Lindstrom (1989), Source waters of the Pacific Equatorial Undercurrent, *Prog. Oceanogr.*, *23*(2), 101–147.
Ueki, I., Y. Kashino, and Y. Kuroda (2003), Observation of current variations off the New Guinea coast including the 1997–1998 El Niño period and their relationship with Sverdrup transport, *J. Geophys. Res.*, *108*(C7), 3243, doi:10.1029/2002JC001611.
Verron, J., and E. Blayo (1996), The no-slip boundary condition and the Gulf Stream separation problem, *J. Phys. Oceanogr.*, *26*(9), 1938–1951.
von Storch, J.-S., C. Eden, I. Fast, H. Haak, D. Hernández-Deckers, E. Maier-Reimer, J. Marotzke, and D. Stammer (2012), An estimate of the Lorenz Energy Cycle for the World Ocean based on the STORM/NCEP simulation, *J. Phys. Oceanogr.*, *42*, 2185–2205. doi:10.1175/JPO-D-12–079.1.
Walker, A., and J. Pedlosky (2002), Instability of meridional baroclinic currents, *J. Phys. Oceanogr.*, *32*(3), 1075–1093.
Wang, G., J. Su, and P. Chu (2003), Mesoscale eddies in the South China Sea observed with altimeter data, *Geophys. Res. Lett.*, *30*, 2121, doi:10.1029/2003GL018532.
Wang, G., D. Chen, and J. Su (2008), Winter eddy genesis in the eastern South China Sea due to orographic wind jets, *J. Phys. Oceanogr.*, *38*, 726–732, doi:10.1175/2007/JPO3868.1.
Xu, Y., and L. L. Fu (2011), Global variability of the wavenumber spectrum of oceanic mesoscale turbulence, *J. Phys. Oceanogr.*, *41*(4), 802–809, doi:10.1175/2010JPO4558.1.
Xu, C., X.-D. Shang, and R. X. Huang (2011), Estimate of eddy energy generation/dissipation rate in the World Ocean from altimetry data, *Ocean Dyn.*, *61*, 525–541, doi:10.1007/s10236- 011-0377-8.
Yu, X., and M. J. McPhaden (1999), Seasonal variability in the equatorial Pacific, *J. Phys. Oceanogr.*, *29*, 925–947.
Zhai, X., H. L. Johnson, and D. P. Marshall (2010), Significant sink of ocean-eddy energy near western boundaries, *Nat. Geosci.*, *9*, 608–612.
Zheng, Q., C.-K. Tai, J. Hu, H. Lin, R.-H., Zhang, F.-C. Su, and X. Yang (2011), Satellite altimeter observations of nonlinear Rossby eddy-Kuroshio interaction at the Luzon Strait, *J. Oceanogr.*, *67*(4), 365–376.